Pressure Induced Amorphization of $Ca(OH)_2$ and GeO_2

Shinji KAWASAKI

OSAKA UNIVERSITY
GRADUATE SCHOOL OF ENGINEERING SCIENCE
DEPARTMENT OF MATERIAL PHYSICS
TOYONAKA OSAKA

Pressure Induced Amorphization of $Ca(OH)_2$ and GeO_2

Shinji KAWASAKI

Synopsis

Precise X-ray diffraction studies have been carried out under high pressure up to 15 GPa for calcium hydroxide ($Ca(OH)_2$) and 21 GPa for α-quartz type germanium oxide (q-GeO_2) in order to clarify structural aspects of the pressure induced amorphization. The pressure variations in X-ray powder diffraction pattern were observed by combining a newly developed X-ray experimental system and a diamond anvil pressure cell. A program software to control the system was originally prepared, which includes many functions such as a determination of setting parameters, a measurement of the diffraction intensity distribution in a reciprocal plane and so on. It was observed that the amorphization of $Ca(OH)_2$ and GeO_2 was reversible and irreversible transition, respectively. The analysis of crystal structure of q-GeO_2 as a function of pressure was performed with single crystal X-ray diffraction data. The amount of the volume change with respect to the transition from a crystalline to an amorphous state was evaluated by in situ optical microscopic (OM) observation under pressure. The elastic wave velocity measurement of high pressure amorphous GeO_2 (a-GeO_2), which was synthesized by the multi-anvil type high pressure apparatus, was also undertaken and the equation of state of a-GeO_2 was determined. It was discovered that there was a discrepancy between the volume of the transformed material from single crystal q-GeO_2 at 6.5 GPa that was evaluated by OM observation and the volume of the synthesized a-GeO_2 at 6.5 GPa that was calculated by the obtained equation of state. This discrepancy was interpreted by the model that two amorphous states existed. The Raman scattering spectrum was measured and the result was consistent with this model.

Contents

§1 Introduction

A) Pressure Induced Amorphization

Non-crystalline materials attract many interests as well as crystalline substance and have an important role in many fields. Non-crystalline materials have some advantages as follows.

1: Physical properties are not restricted to a specific direction, because non-crystalline material is physically isomorphic.

2: Non-crystalline phases in many materials are easily produced.

In spite of the importance mentioned above, there is an ambiguity in classifying the structures of non-crystalline materials. For example, the difference between glass and amorphous is not clear. In order to avoid the ambiguity, in this study the term amorphous is defined to describe a sample that provides no measurable X-ray diffraction peak.

Pressure induced amorphization at ambient temperature was discovered by Fujii et al.[1],[2] and some materials in Table 1-1[3]-[10] were known to be amorphous by compression.

Few general rules for the pressure induced amorphization were found[11]-[14]. Mishima et al.[15],[16] pointed out that the amorphization occurred along the extrapolation of the melting line. However, it has not been sure that every material described in Table 1-1 is transformed to amorphous state under such condition and furthermore, the physical meaning to extrapolate the melting line is not clear.

B) $Ca(OH)_2$

(1) Structural aspect

$Ca(OH)_2$ is an industrially important material. For example, $Ca(OH)_2$ is utilized as material for construction such as Portland cement. The crystal structure of $Ca(OH)_2$ corresponds to the structure of CdI_2 if OH is treated as a single anion (Fig.1-1). Its space group is $P\bar{3}m1$ and it is characterized by sheets of linked $Ca(OH)_6$ octahedra[17].

Recently, it was reported that $Ca(OH)_2$ was transformed from a crystalline to an amorphous state under a high pressure at about 12 GPa and room temperature[8]. However, the detailed mechanism of the amorphization is still unknown.

(2) Analogy of $Mg(OH)_2$

The structure of $Mg(OH)_2$ is also CdI_2 type. Both Ca and Mg are alkaline-earth metal elements. Since the ionic radius of Mg is smaller than Ca, structural change is expected to be found under high pressures in $Mg(OH)_2$ if it occurs. The behavior of $Mg(OH)_2$ under high pressure is, however, interesting from the earth scientific point of view, because $Mg(OH)_2$ is one of the H_2O reservoirs within the earth's mantle. Therefore, dehydration of $Mg(OH)_2$ under high pressure is

one of the themes for earth science[18].

C) GeO_2

(1) Structural aspect

There are two stable polymorphs (α-quartz and rutile types) of GeO_2 (Fig.1-2)[19]. For convenience sake, α-quartz type and rutile type GeO_2 are abbreviated to q-GeO_2 and r-GeO_2, respectively. As shown in Fig.1-3, q-GeO_2 is stable under high temperature at ambient pressure. However, q-GeO_2 can be metastably quenched under room condition.

The space group of q-GeO_2 and r-GeO_2 is $P3_121$ and $P4_2/mnm$, respectively[20],[21],[22]. The structure of q-GeO_2 is characterized by a GeO_4 tetrahedral framework system and a germanium atom is coordinated by four oxygen atoms. On the other hand, a germanium atom in r-GeO_2 is surrounded by six oxygen atoms in distorted octahedral coordination. This polymorph is dense compared with q-GeO_2 and the density of q-GeO_2 and r-GeO_2 is 4.2 and 6.3 g/cm^3, respectively.

(2) Analogy of SiO_2

GeO_2 has a crystal chemical analogy of SiO_2[23]. Both GeO_2 and SiO_2 have α-quartz type and rutile type polymorphs. α-quartz (SiO_2) is one of the major component minerals in the earth's mantle. We could not understand the phenomena in the earth's mantle without the knowledge of the behavior of SiO_2 under high pressure.

Recently, it was reported that α-quartz (SiO_2) was transformed from a crystalline to an amorphous state between 25-30 GPa at room temperature[3]. However, the detailed mechanism of the amorphization of α-quartz is still unknown. The transition pressure is a little too high for several experiments such as X-ray single crystal experiment. On the other hand, the amorphization of GeO_2 occurs at about 6.5 GPa which is in the region possible to perform several experiments[24],[25]. To investigate the amorphization of q-GeO_2 gives hints to understand that of α-quartz. From this time forward, the high pressure amorphous GeO_2 is abbreviated to a-GeO_2 for convenience.

D) X-ray Scattering Study for the Structural Transition

X-ray scattering is recognized as the most powerful tool available for the study of the structural transition of solids, because X-ray diffraction pattern is related directly to the structural symmetry. The in situ X-ray observation has been undertaken at various temperatures and pressures. For such observation, a temperature and/or pressure controller is installed in the X-ray experimental instrument.

The information concerning not only long range order such as crystal symmetry but also short range order is acquired by the observation of X-ray diffuse scattering[26]. To understand the dynam-

ics of the structural transition, we need to know the short range order that is affected by nuclei and embryo in the process of crystallization[27].

However, we can hardly get intense signal in the case mentioned above, because the intensity of the diffuse scattering is almost one-hundredth that of the diffraction and the sample space is often limited when some devices are used for the intensity measurement under the desired physical condition.

The object field for X-ray scattering study would be expected to be wide if weak signal could be detected effectively.

As mentioned above, to investigate the behavior of $Ca(OH)_2$ and q-GeO_2 under high pressure is important both industrially and earth scientifically. A main purpose of this investigation is to clarify the structural aspects of the pressure induced amorphization of $Ca(OH)_2$ and q-GeO_2. Further, the development of the new X-ray experimental system for getting an excellent X-ray scattering spectrum is also one of our purposes.

Table1-1 Amorphization pressure of some materials

Material	Amorphization Pressure (GPa)
SnI_4	10
SiO_2(α-quartz)	25-30
SiO_2(coesite)	30-34
$AlPO_4$	15
$LiKSO_4$	13
$CaAl_2Si_2O_8$	22-28
Fe_2SiO_4	39
$Ca(OH)_2$	12
GeO_2	6.5

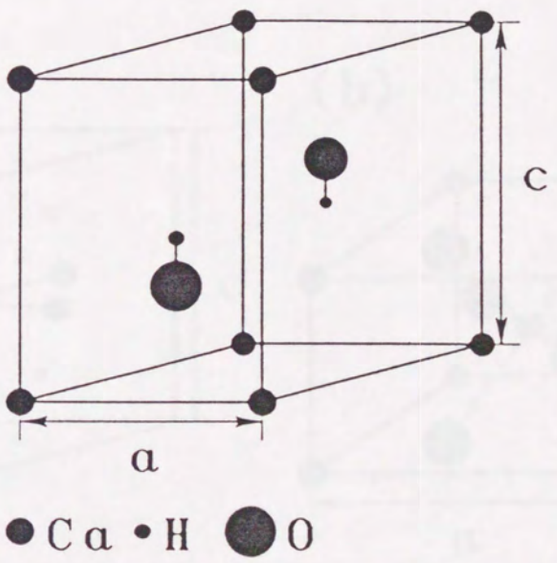

Fig.1-1 Crystal structure of $Ca(OH)_2$

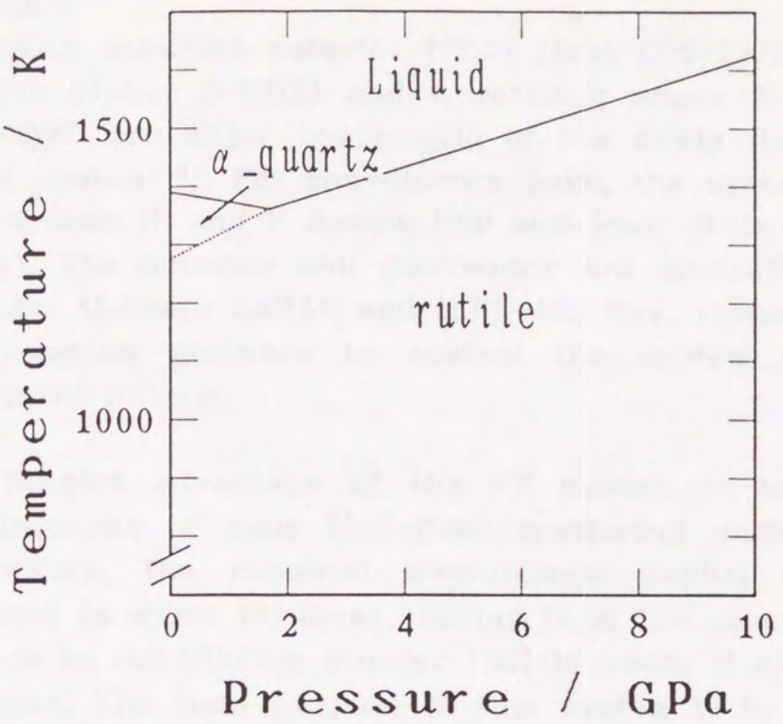

Fig.1-2 P-T phase diagram of GeO_2

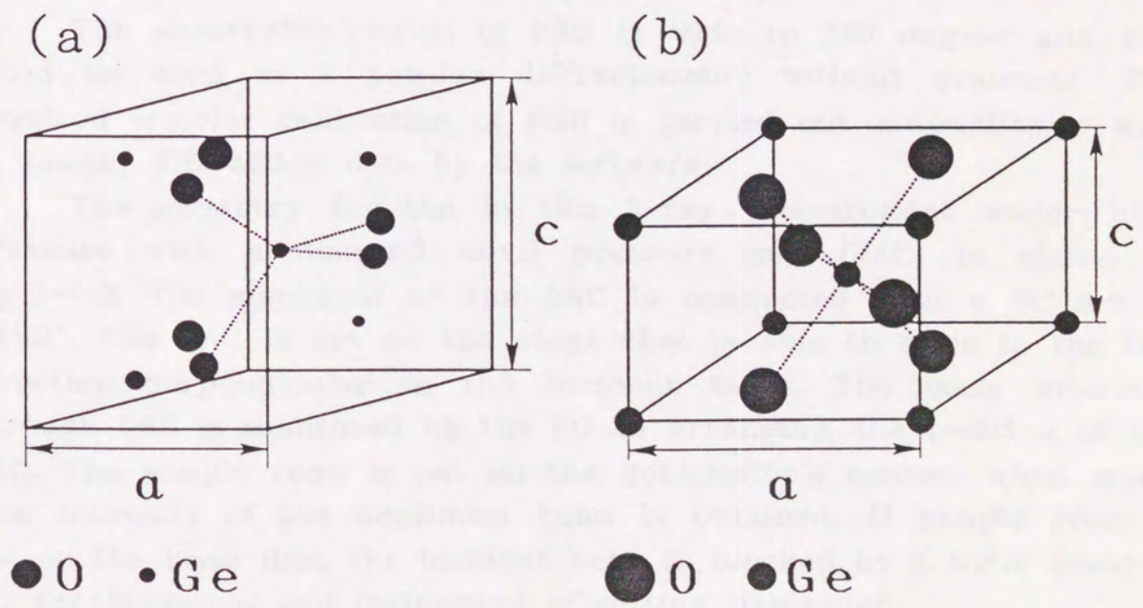

Fig.1-3(a),(b) Crystal structure of GeO_2 (a) α-quartz type (b) rutile type

§2 Experimental

§2-1 Newly Developed X-ray Experimental System

A) Specification

A position sensitive detector (PSD) (Inel CPS-120), a four-circle diffractometer (Huber D-8219) and a rotating anode X-ray generator (Rigaku RU-200) are major components of the newly developed X-ray experimental system[28]. For convenience sake, the system is abbreviated to PF system (P and F denote PSD and four-circle diffractometer, respectively). The detector and goniometer are controlled by a personal computer through CAMAC and IEEE-488 bus, respectively (Fig.2-1-1). The program software to control the system was originally prepared by the author.

B) Purpose

The biggest advantage of the PF system is to observe the scattering intensity of many (512-4096) scattering vectors simultaneously. Therefore, the required measurement period when the PF system is used is about 10^3 times shorter than the case when a point detector such as scintillation counter (SC) is used, if all other conditions are same. The main purpose of this system is to get high S/N ratio for weak signal (e.g. in the case of the in situ X-ray experiment under high pressure) in a short time.

C) Functions

Functions as follows could be executed by using the software.

(1) Powder diffractometer

The observable region of PSD is wide to 120 degree and PSD could be used as a powder diffractometer without scanning. The required angular calibration of PSD is carried out automatically with Si powder diffraction data by the software.

The geometry for the in situ X-ray measurement under high pressure with a diamond anvil pressure cell (DAC) is shown in Fig.2-1-2. The alignment of the DAC is conducted with a SC set at $2\theta=0°$. The DAC is set on the stage that is able to move in the two direction perpendicular to the incident beam. The beam intensity through DAC is monitored by the SC as arranging the position of the DAC. The sample room is set on the goniometer's center, when maximum intensity of the monitored beam is obtained. If sample room is not on the beam line, the incident beam is blocked by a metal gasket.

(2) Establishment and refinement of setting parameter

In the single crystal X-ray experiment, the setting parameter must be known in prior to all other measurements[29]. Establishment and refinement of setting parameter are carried out in this system as a following procedure.

1: Some reciprocal points near origin are searched by the ω, χ, ϕ rotation.

2: Determination of setting parameter is made by the vector minimum method[30] with the coordinates of those points.

3: Reflections having appointed hkl indices are observed and the coordinates of the reciprocal points are determined.

4: The setting parameters are refined by least square method with the appointed hkl indices and the observed coordinates.

(3) ω-sweep mode

One of the weak points of single crystal X-ray diffraction measurement is to need the 2θ, ω, χ, ϕ rotation drives for individual reflection. Therefore, it takes a considerably long measurement time to collect diffraction intensities of reflections large enough for the structure analysis. PF system makes it possible to do so with single crystal as a following procedure (named "ω-sweep mode").

1: A reciprocal plane involving an origin is moved in a horizontal plane (a detector plane) by combining the ϕ and χ rotations (see Appendix 1).

2: Counting of scattering photons is carried out with ω continuous scanning.

Fig.2-1-3 is an example of the data observed by this function. It looks like a powder diffraction pattern and four peaks (five reflections) were detected. ω-sweep mode needs only a simple movement (ω rotating) and some reflections could be observed for a short time. For a sample having simple symmetry, lattice constants can be easily determined by using this method.

We could get the scattering intensity distribution in the reciprocal plane only by changing the ω continuous scanning to the step scanning in the procedure 2 mentioned above. Therefore, the measurements of diffuse scattering and/or supper-lattice reflection could be performed easily (see §2-3-(C)).

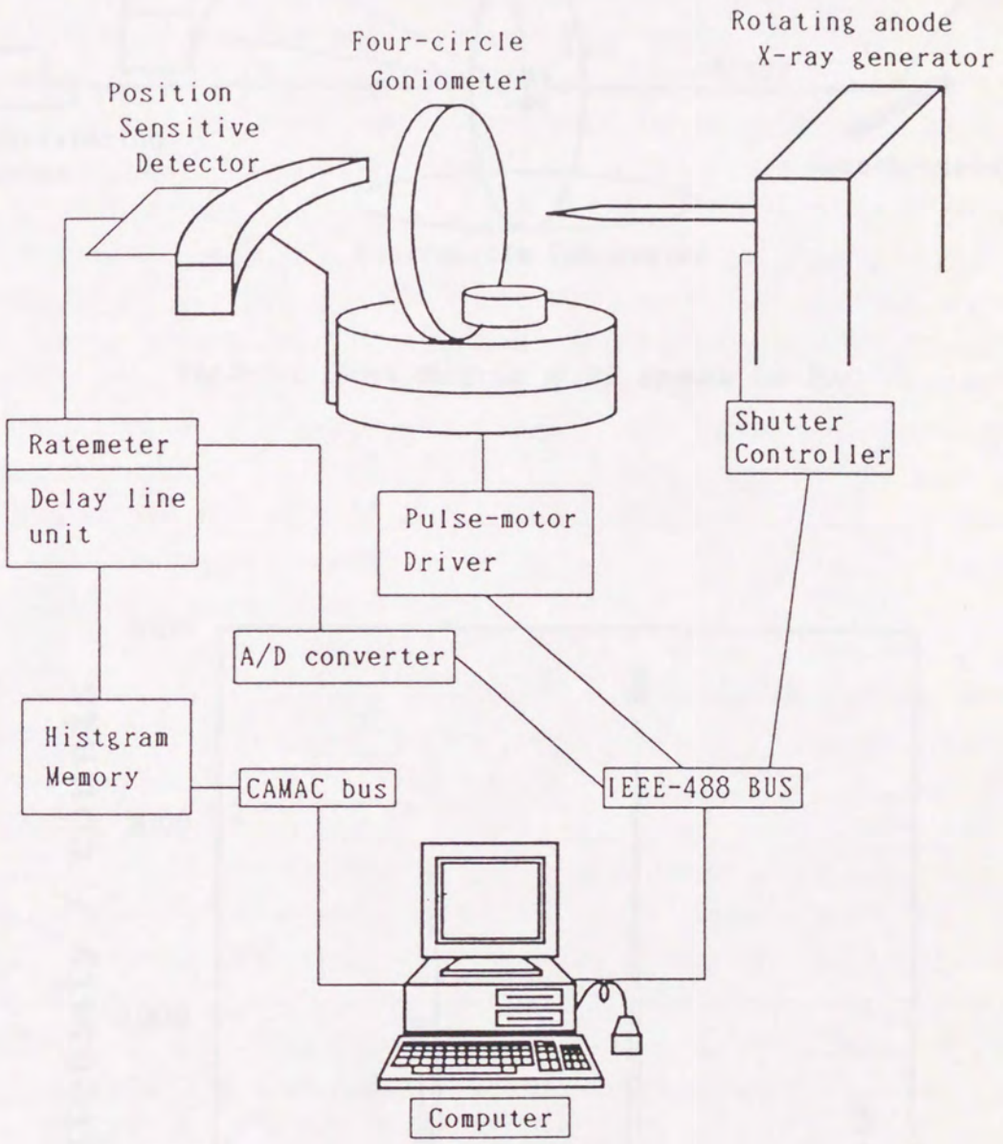

Fig.2-1-1 Block diagram of PF system

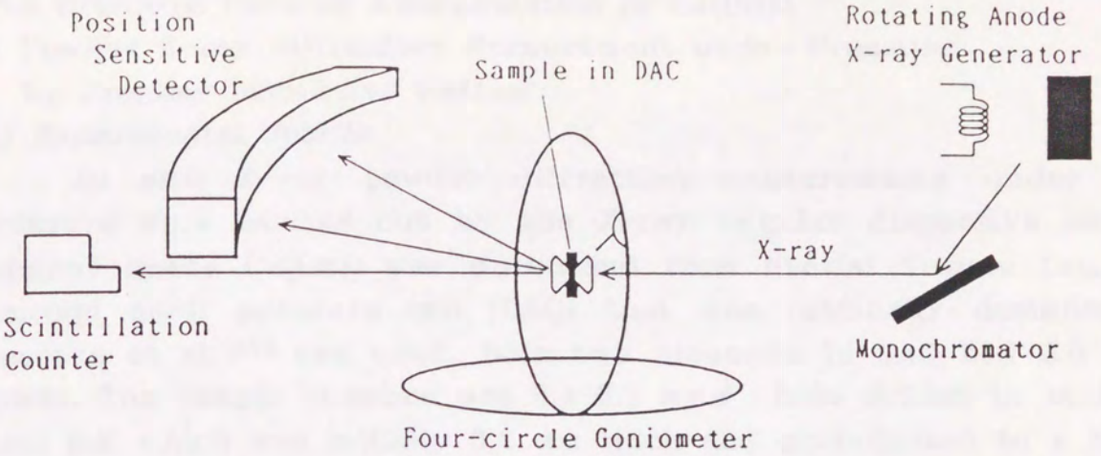

Fig.2-1-2 Block diagram of PF system for DAC

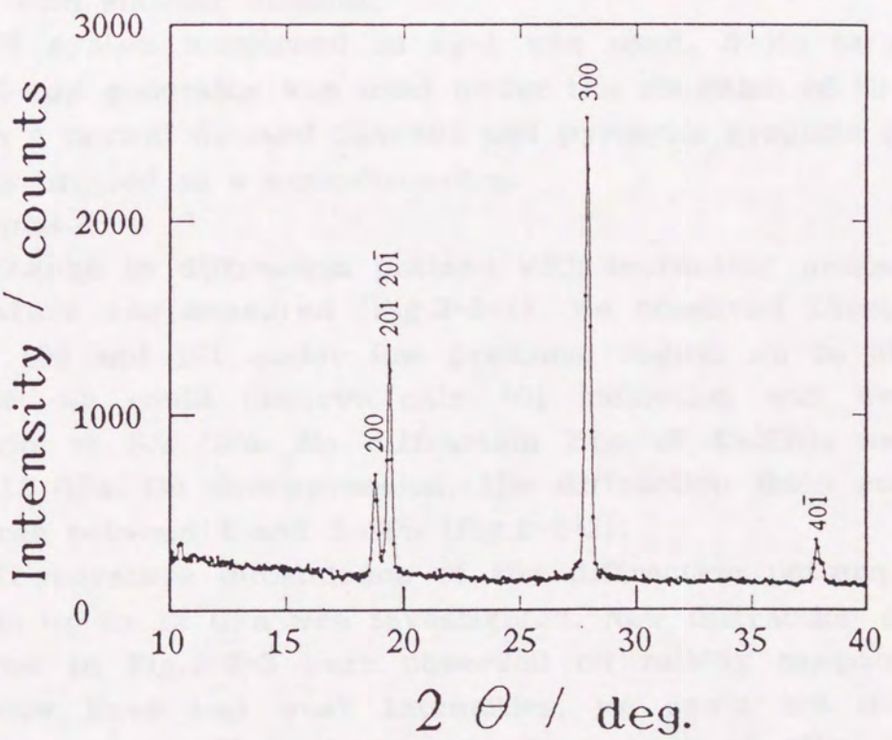

Fig.2-1-3 Observed diffraction lines of $LiKSO_4$ single-crystal by ω-sweep mode. ω rotation was driven at a speed of 0.1°/second for 300 seconds.

§2-2 Pressure Induced Amorphization of $Ca(OH)_2$

A) Powder X-ray Diffraction Measurement under Pressure by Angular Dispersive Method

(1) Experimental details

In situ X-ray powder diffraction measurements under high pressure were carried out by the X-ray angular dispersive method. Reagent grade $Ca(OH)_2$ was purchased from Nacalai Tesque Inc. The diamond anvil pressure cell (DAC) that was originally designed by Yamaoka et al.[31] was used. Both two diamonds in DAC had 0.5 mmϕ culets. The sample chamber was 0.1-0.2 mmϕ hole drilled in stainless steel foil which was initially 0.2 mm thick and preindented to a thickness of about 0.1 mm. The mixture of methanol : ethanol = 4 : 1 was used as a pressure transmitting medium (PTM)[32]. Pressure was determined by the shift of R_1 fluorescence line of ruby[33],[34].

In case of the experiment under high temperature and pressure, internal sample of NaCl was used as a pressure gauge and no liquid PTM was used. Ni-Cr ring heater was installed around one of the two diamonds. Temperature was measured by a Pt-Pt/Rh13% thermocouple contact with another diamond.

PF system mentioned in §2-1 was used. A Mo target rotating anode X-ray generator was used under the condition of 50 kV and 150 mA with a normal focused filament and pyrolytic graphite (002) reflection was utilized as a monochrometor.

(2) Results

Change in diffraction pattern with increasing pressure at room temperature was measured (Fig.2-2-1). We observed three reflections of 001, 100 and 101 under low pressure region up to about 7 GPa. However, we could observe only 101 reflection and weakened 100 reflection at 9.7 GPa. No diffraction line of $Ca(OH)_2$ was observed above 12 GPa. On decompression, the diffraction lines reappeared at pressures between 4 and 2 GPa (Fig.2-2-2).

Temperature dependence of the diffraction pattern after compression up to 12 GPa was investigated. New diffraction lines marked by arrow in Fig.2-2-3 were observed on raising temperature. Since these new lines had weak intensities, we could not determine the crystal structure. Those lines were also observed after quenched to room temperature under the compressed condition (Fig.2-2-4). As decreasing pressure to 1 GPa, the diffraction lines of starting material reappeared. The new lines appeared on heating were also observed at 1 GPa. However, these lines disappeared on decompression to atmospheric pressure.

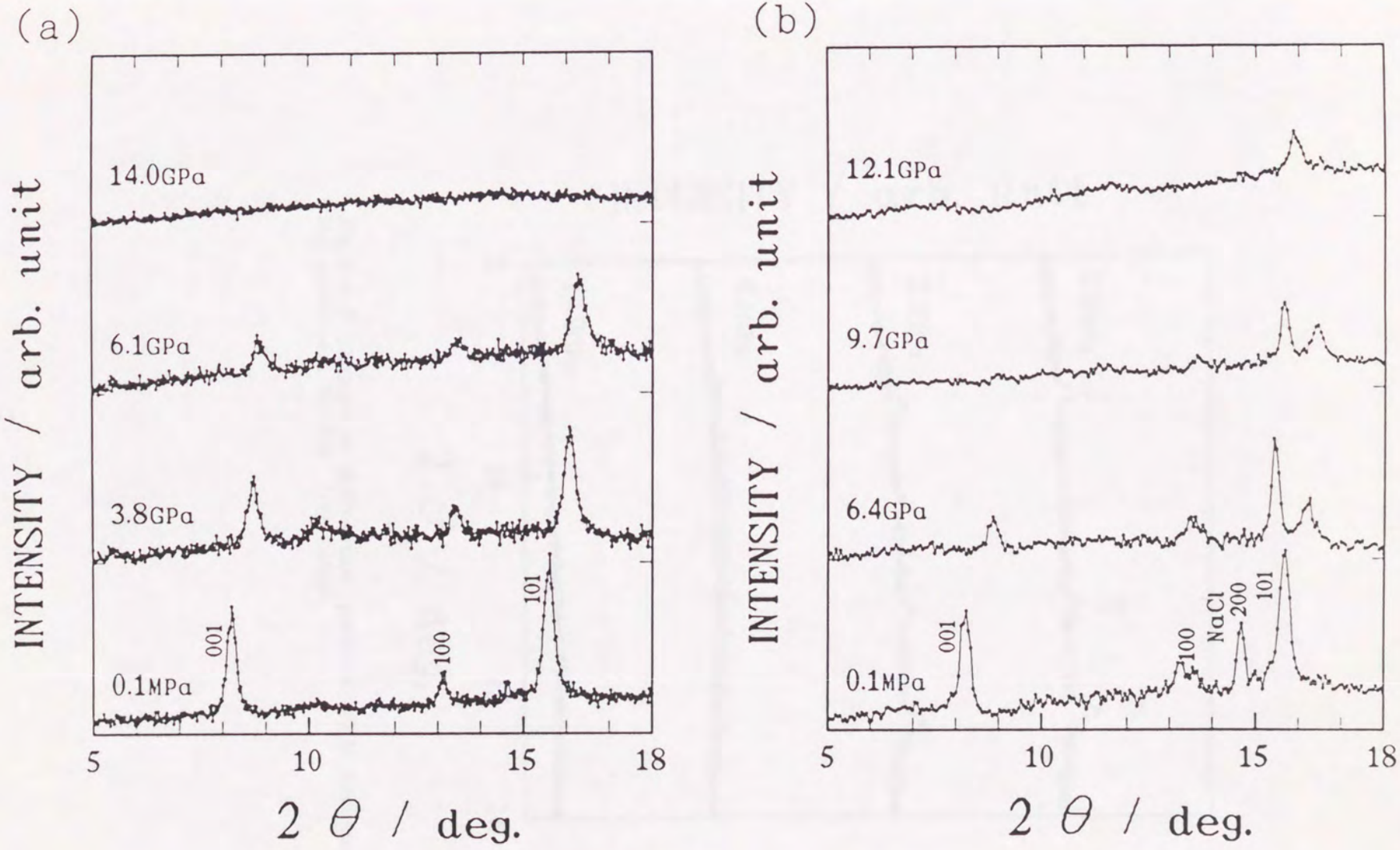

Fig.2-2-1(a),(b) Change in diffraction pattern with increasing pressure. Mo Kα irradiated. (a) The mixture of methanol : ethanol = 4 : 1 was used as a PTM. (b) Internal sample of NaCl was used as a pressure gauge.

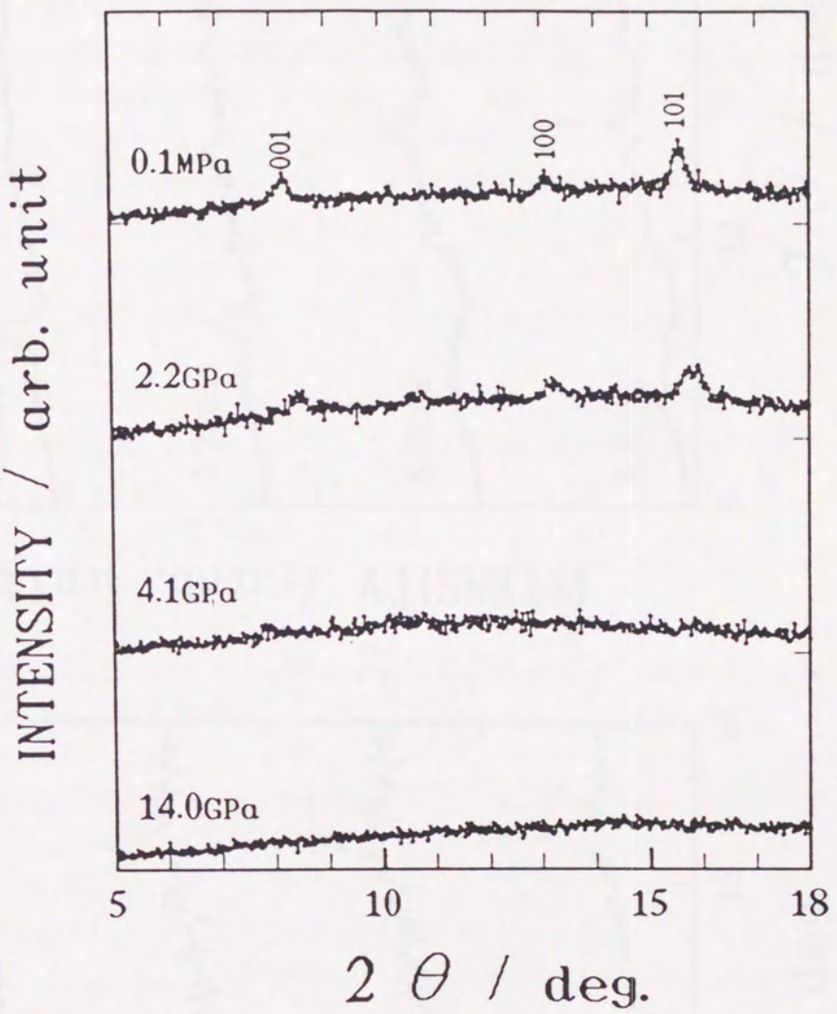

Fig.2-2-2 Change in diffraction pattern with decreasing pressure. Mo Kα irradiated.

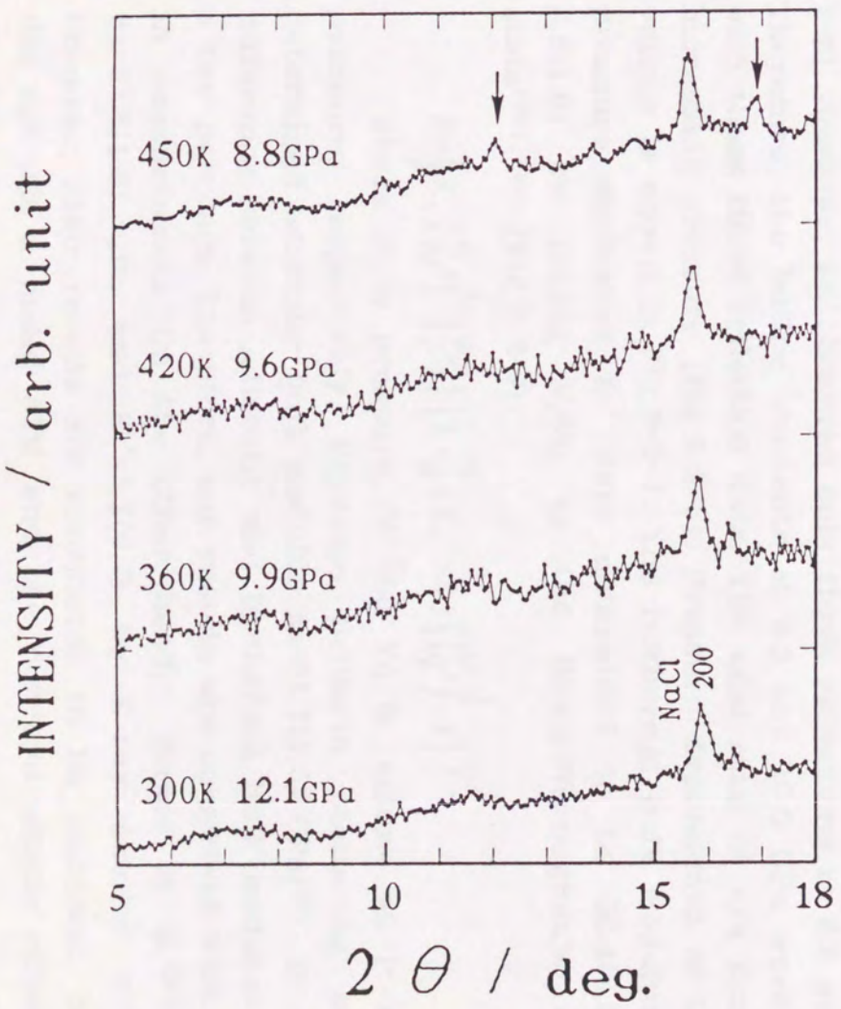

Fig.2-2-3 Change in diffraction pattern with raising temperature. Mo Kα irradiated.

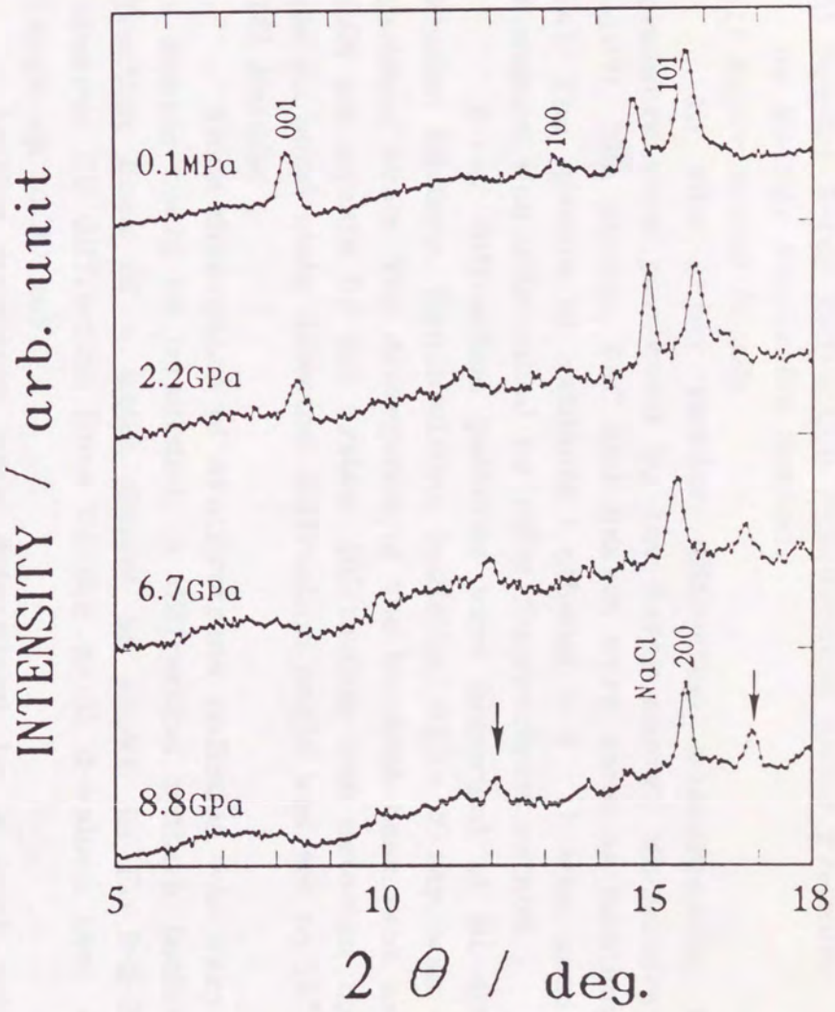

Fig.2-2-4 Change in diffraction pattern with decreasing pressure after heating.

B) Powder X-ray Diffraction Measurement under Pressure by Energy Dispersive Method

(1) Experimental Details

In situ X-ray powder diffraction measurements under high pressure were performed by the X-ray energy dispersive (ED) method[35]. The sample, DAC and gasket were same as mentioned in §2-2-(A). The mixture of methanol : ethanol = 4 : 1 was used as a PTM. Pressure was determined by ruby fluorescence method.

X-ray diffraction patterns were observed at BL-4B station of Photon Factory. Synchrotrons radiation white X-ray was used as an incident beam. The divergence of the incident beam was as small as a 0.08 mm square by slit system. Diffraction was detected by an intrinsic Ge solid state detector. Diffraction angle was set to 16°.

(2) Results

Since divergence of synchrotrons radiation was very small, only a sample could be irradiated. A diffraction pattern included no diffraction lines of a metal gasket as shown in Fig.2-2-5. We could observe ED diffraction lines having small d-values that were in the range up to 30 keV.

Lattice constants were determined by a least square method with six observed 001,100,111,102,110,101 reflections (Table2-2-1, Fig.2-2-6). However, we observed only three reflections at 8.5 and 10.0 GPa. Therefore, the lattice constants at 8.5 and 10.0 GPa were determined with those three reflection data. The axial ratio of c/a decreased with increasing pressure (Fig.2-2-6). Pressure dependence of the unit cell volume is shown in Fig.2-2-7. The isothermal bulk modulus K_t and its pressure derivative K_t' were determined to be 30.4(2.9) GPa and 8.6(1.8) by fitting V/Vo to the Birch-Murnaghan's equation of state[36],[37] (Fig.2-2-7).

$$P=\frac{3}{2}K_t\left\{\left(\frac{V_0}{V}\right)^{\frac{7}{3}}-\left(\frac{V_0}{V}\right)^{\frac{5}{3}}\right\}\left[1+\frac{3}{4}(K_t'-4)\left\{\left(\frac{V_0}{V}\right)^{\frac{2}{3}}-1\right\}\right]$$

where P is pressure, V and Vo is volume at P and ambient pressure, respectively. Previous Brillouin scattering measurements determined adiabatic bulk modulus K_s=31.7(2.5) GPa[38]. In general, the difference between adiabatic and isothermal bulk modulus falls within a few percents. Therefore, our results are consistent with the Brillouin measurements. On the other hand, Meade et al.[39] determined K_t=37.8(1.8) GPa and K_t'=5.2(0.7) by X-ray powder diffractometry. However, their results are considered to be incorrect, because they did not use a liquid PTM and the non-hydrostatic effect should be considered.

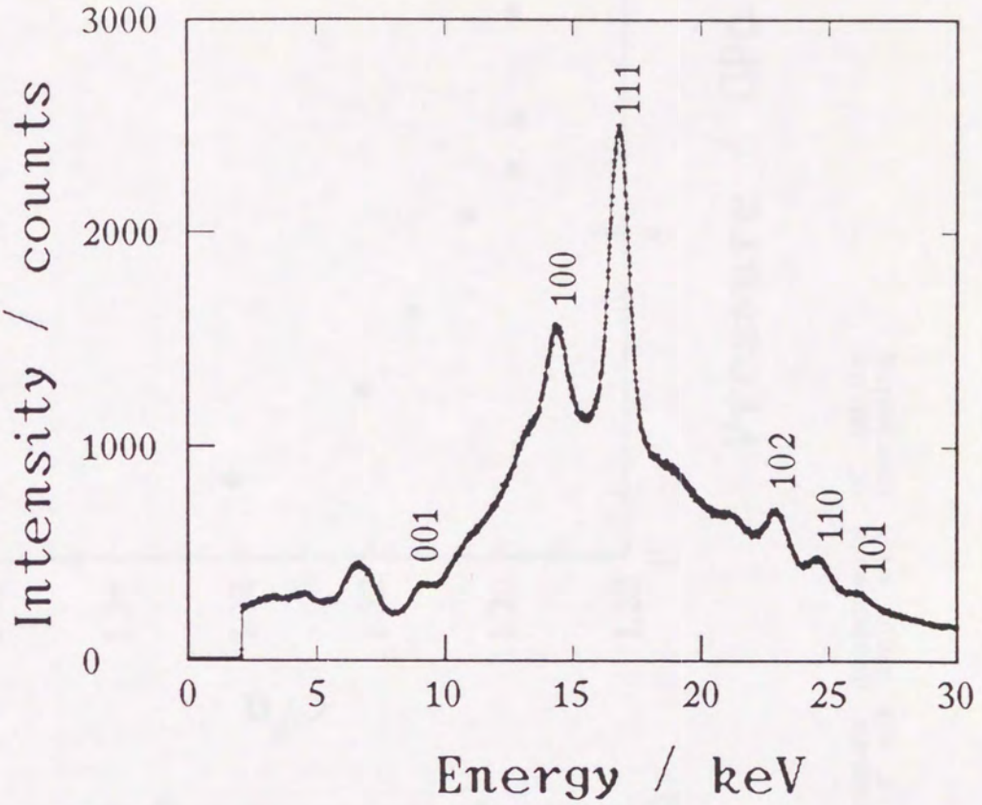

Fig.2-2-5 Observed ED spectrum of $Ca(OH)_2$ in DAC.

Table2-2-1 Lattice constants as a function of pressure for $Ca(OH)_2$

P (GPa)	a (nm)	c (nm)
1.2	0.3581(0.0001)	0.4804(0.0004)
2.6	0.3557(0.0002)	0.4699(0.0006)
3.8	0.3534(0.0001)	0.4642(0.0003)
5.3	0.3520(0.00002)	0.4592(0.00005)
6.0	0.3509(0.0001)	0.4553(0.0003)
6.8	0.3498(0.0001)	0.4537(0.0002)
8.5	0.3471(0.0005)	0.4504(0.0012)
10.0	0.3475(0.0006)	0.4457(0.0017)

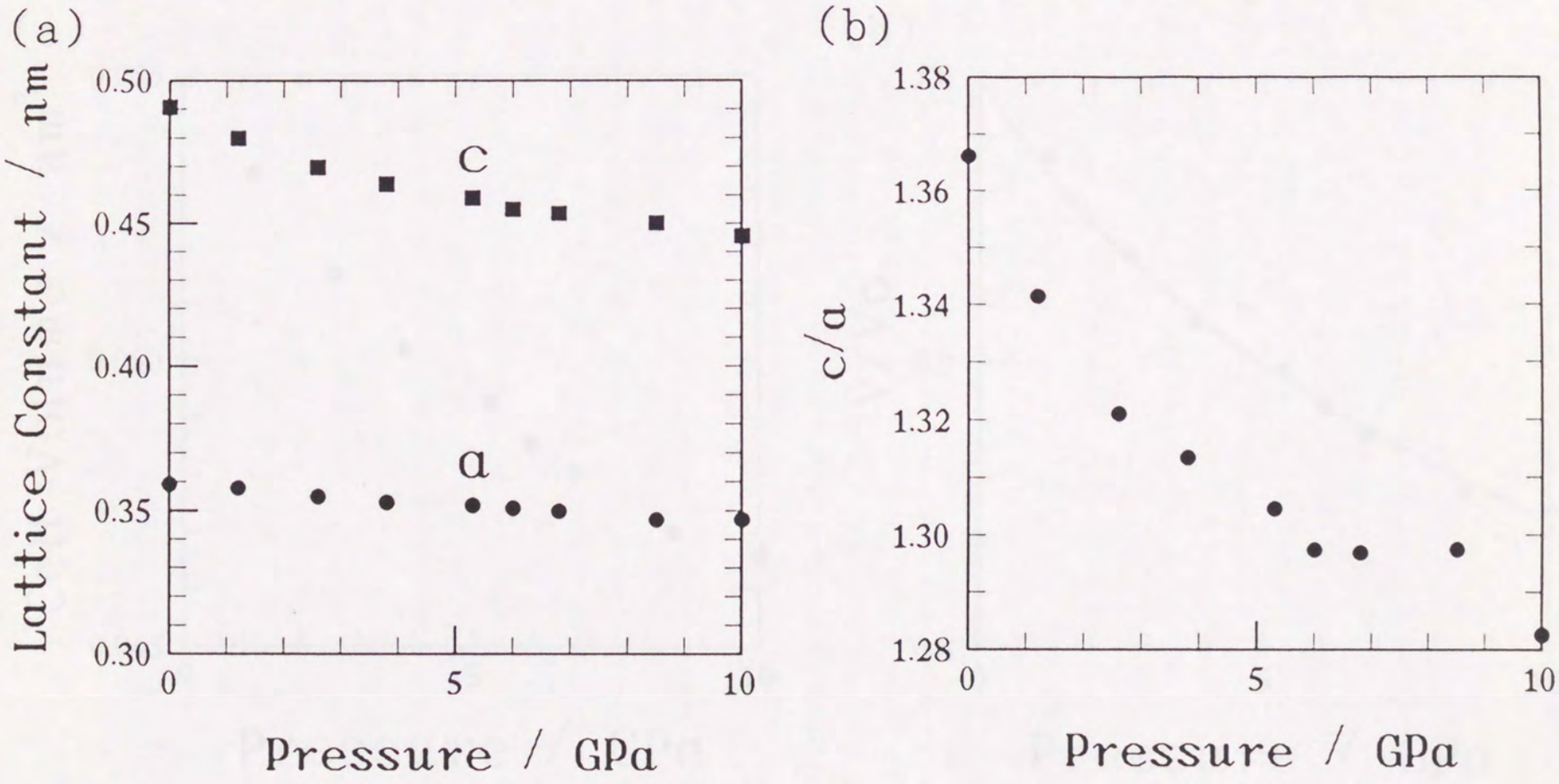

Fig.2-2-6(a),(b) (a) Pressure dependence of lattice constants. (b) Change of c/a ratio with increasing pressure.

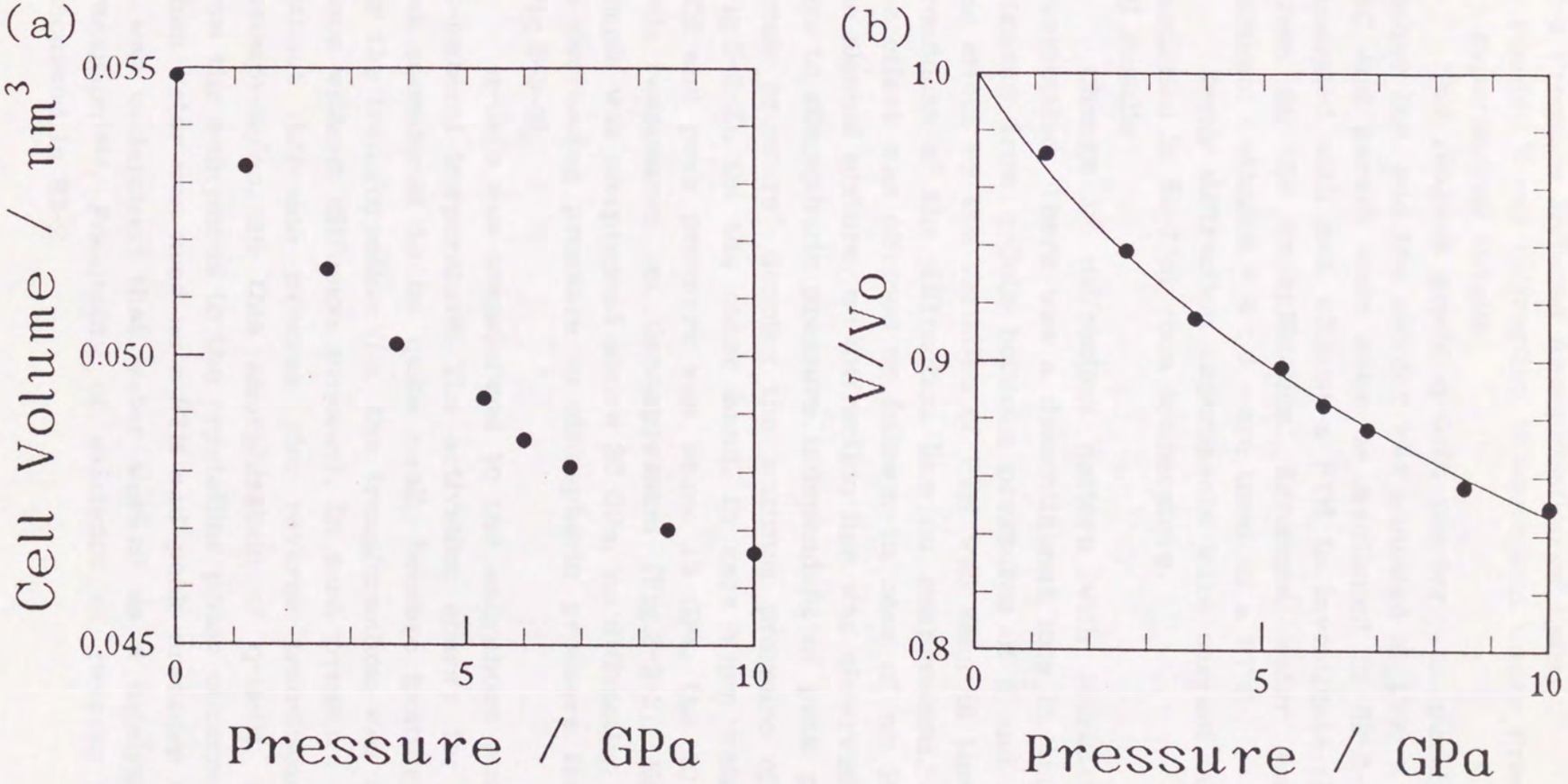

Fig.2-2-7(a),(b) (a) Pressure dependence of unit cell volume. (b) Change of V/Vo ratio with increasing pressure. Solid curve is fitted to the Birch-Murnaghan's equation of state.

§2-3 Pressure Induced Amorphization of GeO_2

A) Powder X-ray Diffraction Measurement under Pressure

(1) Experimental Details

The reagent grade q-GeO_2 powder was purchased from Nacalai Tesque Inc. and the powder was annealed at 1200 K for 24 hours. The DAC and gasket were same as mentioned in §2-2-(A). Pressure was generated with and without a PTM to investigate the effect of shear stress on the amorphization. Kerosene, water and the mixture of methanol : ethanol = 4 : 1 were used as a PTM.

X-ray diffraction experiments were carried out with PF system mentioned in §2-1 at room temperature.

(2) Results

Change in diffraction pattern with increasing pressure was investigated. There was a discontinuous loss in the diffracted X-ray intensity from q-GeO_2 between pressures of 6 and 8 GPa (Fig.2-3-1). The effect by the variation of PTM was seen in the difference of the broadness of the diffraction line on compression. On decompression, the effect was obvious as follows. In case of no PTM, kerosene and the alcohol mixture, no diffraction line was observed after decompression to atmospheric pressure independent of peak pressure (the term "peak pressure" denotes the maximum pressure of each experiment) (Fig.2-3-2). On the other hand, in case when water was used as a PTM and peak pressure was below 15 GPa, the 101 reflection of q-GeO_2 reappeared on decompression (Fig.2-3-3). However, after the sample was compressed above 20 GPa, no diffraction line was observed as decreasing pressure to atmospheric pressure independent of PTM (Fig.2-3-3).

q-GeO_2 was transformed to the amorphous state by compression at ambient temperature. The activation energy for the amorphization was considered to be quite small, because heating was unnecessary for the transformation (i.e. the transformation was considered to take place without diffusion process). In most pressure induced transition without diffusion process, the reverse transition takes place on decompression. In this amorphization of q-GeO_2, reverse transition from the amorphous to the crystalline phase occurred only in the case when water was used as a PTM and peak pressure was below 15 GPa. It was understood that water worked as a catalyst for the reverse transition[40]. Possibility of existence of reverse transition will be discussed in §3-2.

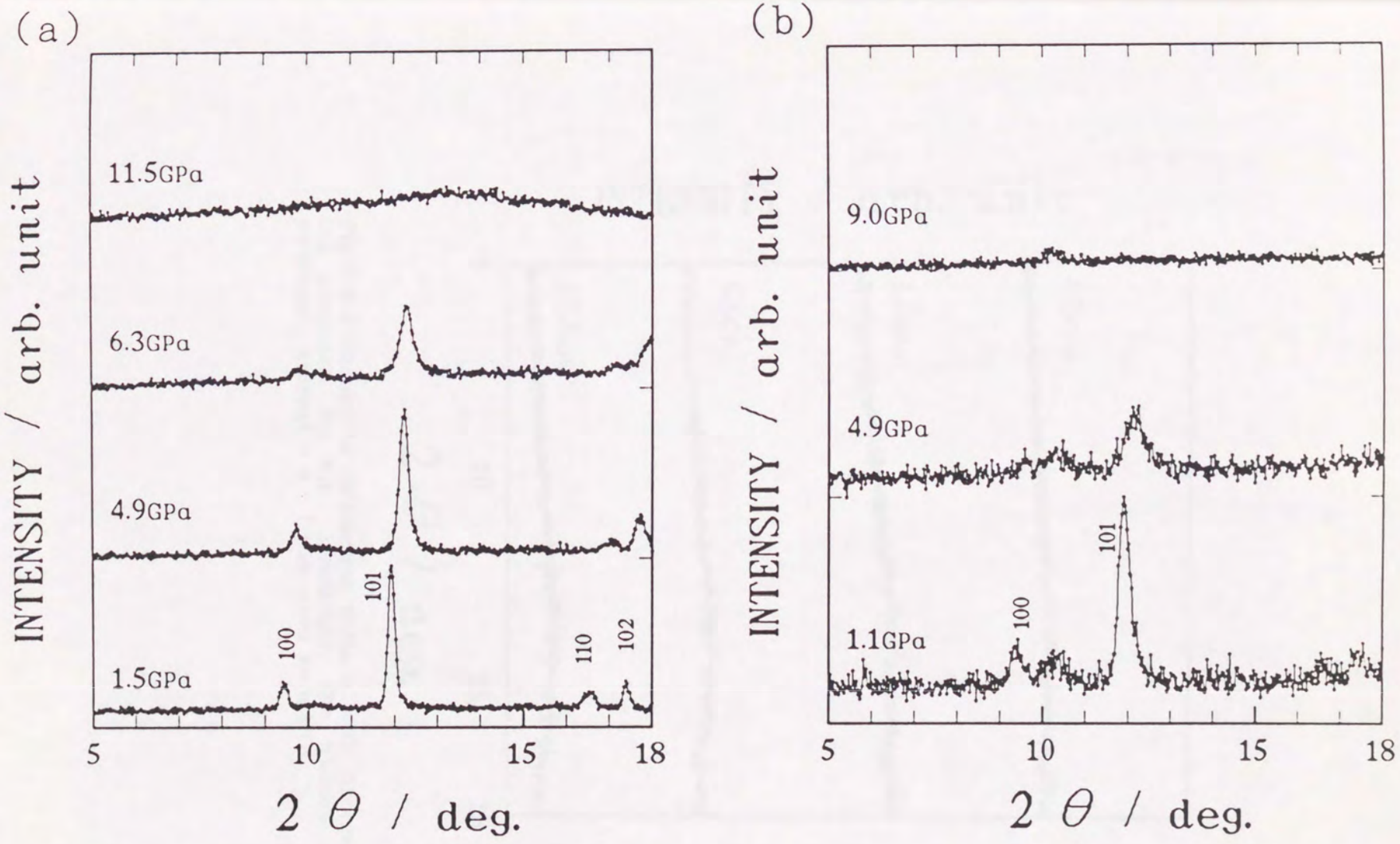

Fig.2-3-1(a),(b) Change in diffraction pattern with increasing pressure. Mo Kα irradiated. (a) Water was used as a PTM. (b) No PTM was used.

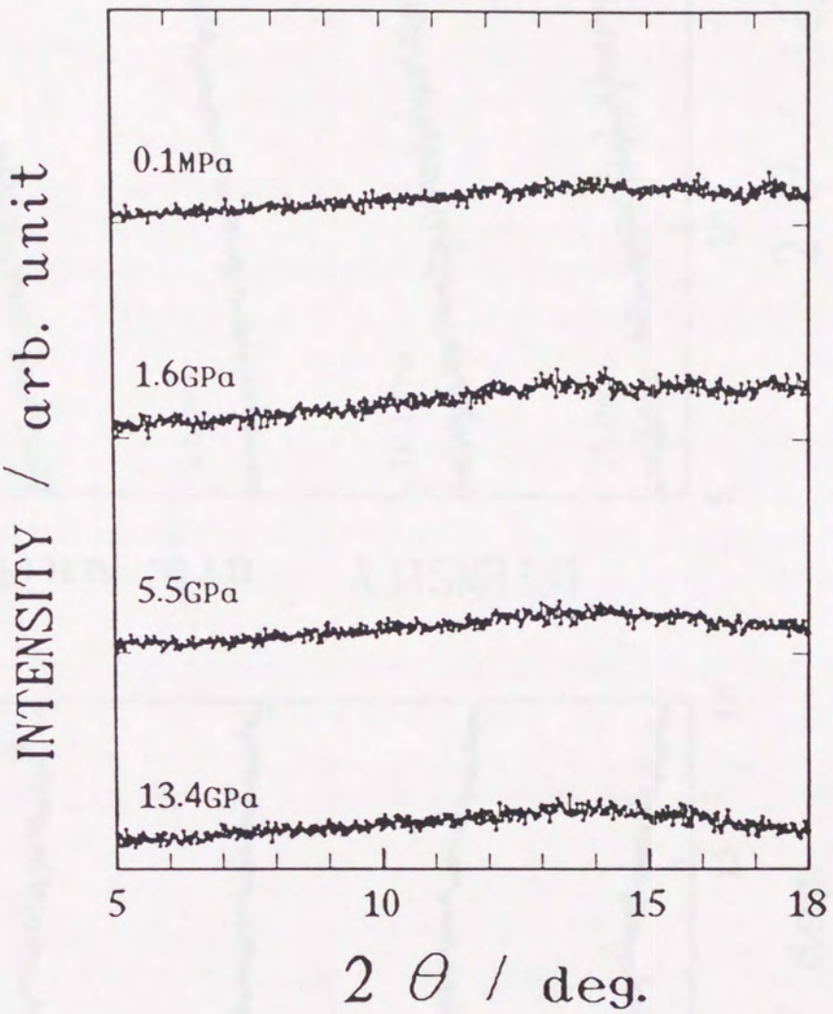

Fig.2-3-2 Change in diffraction pattern with decreasing pressure. Mo Kα irradiated. The mixture of methanol : ethanol = 4 : 1 was used as a PTM.

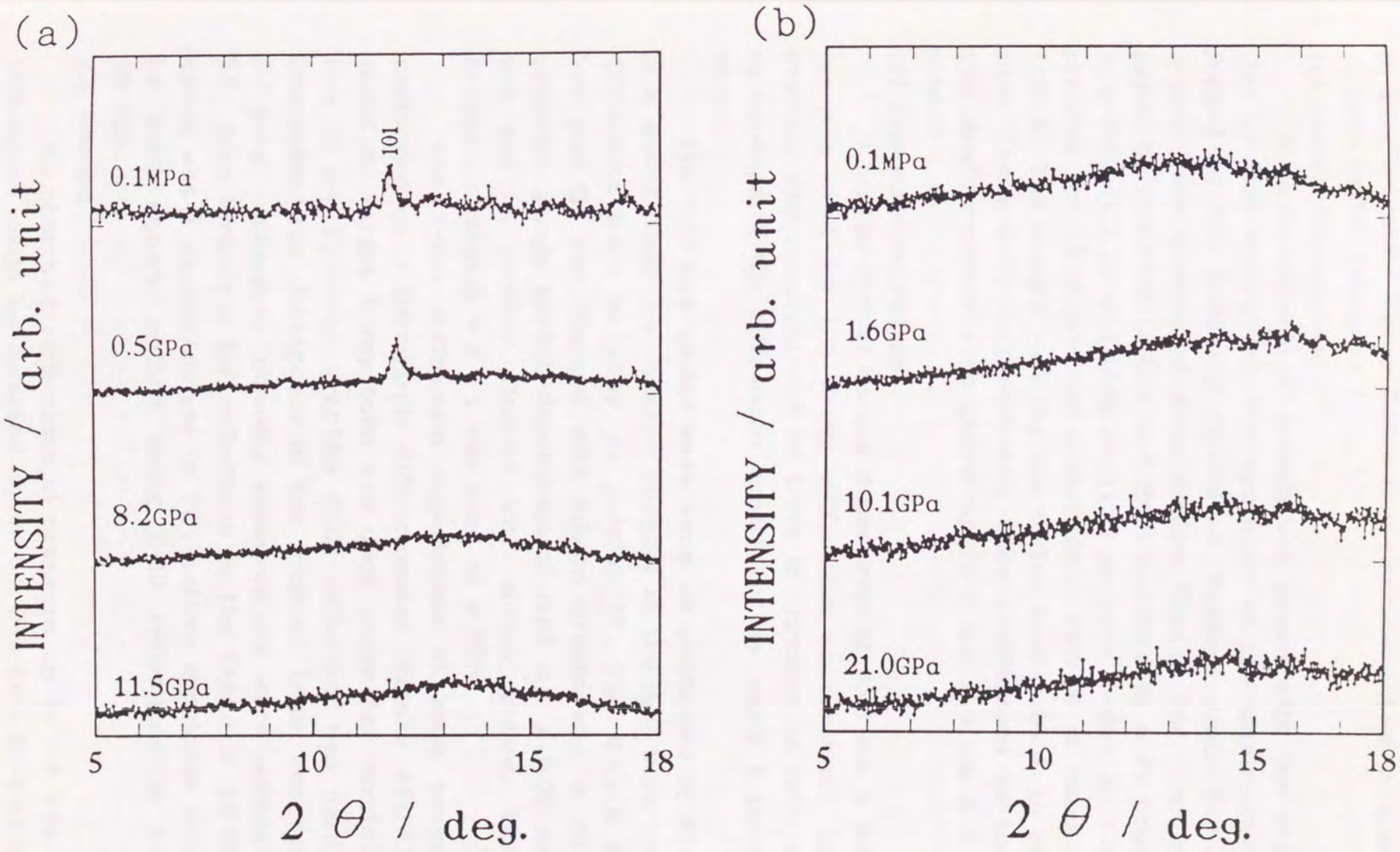

Fig.2-3-3(a),(b) Change in diffraction pattern on decompression from 11.5 GPa (a) and 21.0 GPa (b). Water was used as a PTM. Mo Kα irradiated.

B) Single-Crystal X-ray Diffraction Measurement of α-quartz type GeO_2 under Pressure I

(1) Sample Preparation

A single-crystal of q-GeO_2 was grown with the aid of $Li_2Mo_2O_7$ flux by slow cooling[41]. The synthesis of the single-crystal was performed by the following procedure. Reagent grade Li_2CO_3, MoO_3 and q-GeO_2 were purchased from Nacalai Tesque Inc. $Li_2Mo_2O_7$ was prepared by reacting Li_2CO_3 and MoO_3 powders in a Pt crucible at 1100 K. q-GeO_2 (1.0 g) and $Li_2Mo_2O_7$ (11.5 g) were heated to 1400 K in a Pt crucible for 12 hours and cooled from 1400 K at rates 3 K/hour to 1100 K. The sample was rapidly cooled from 1100 K to room temperature. The q-GeO_2 single-crystals were synthesized in the flux glass. The single crystals were grown up to 5 mm x 5 mm x 3 mm at maximum.

(2) Experimental Details

A single-crystal having dimensions of 0.08 mm x 0.08 mm x 0.03 mm was used for the X-ray diffraction measurement. Quality of the crystals was examined and no trace of existence of twin was confirmed in advance of the diffraction experiment by using a polarizing microscope.

The DAC and gasket were same as mentioned in §2-2-(A) Beryllium mount disks for diamond support in the DAC were used to collect diffraction lines as many as possible[42]. The q-GeO_2 single-crystal was put on the diamond with silicon grease and a ruby tip as a pressure gauge having dimensions of 0.02 mm x 0.02 mm x 0.01 mm was put on another diamond with silicon grease. The mixture of methanol : ethanol = 4 : 1 was used as a PTM.

The X-ray diffraction experiments at room temperature were performed on a four-circle diffractometer (Rigaku AFC-6). A conventional Mo target X-ray tube was used under the condition of 35 kV and 30 mA. Pyrolytic graphite (002) reflection was used as a monochrometor. The divergence of the incident beam was controlled in a 0.8 mmϕ collimator. Intensity measurements were carried out with ω-2θ scan technique for reflections in the range of $2\theta < 50°$. The scan speed was 1 degree/minute in 2θ. Lattice constants were determined by least square method using 8-10 reflections in the range of $30° < 2\theta < 40°$.

(3) Results

We observed reflections at pressure up to 5.8 GPa. However, no reflections could be detected above 6.5 GPa (see §2-3-(D)).

The pressure dependence of lattice constants was investigated (Table2-3-1, Fig.2-3-4). The axial ratio of c/a increased with increas-

ing pressure (Fig.2-3-4). The isothermal bulk modulus K_t was determined by fitting V/Vo to the Birch-Murnaghan's equation of state. We determined K_t=32.7(3.3) GPa and K_t'=6.0(2.2) (Fig.2-3-5). Based on the assumption that K_t'=4, the value of K_t was determined to be 36.0(0.8) GPa. The determined value is smaller than K_t=39.0 GPa (K_t'=4.0) determined by Sowa et al.[14] with X-ray single crystal diffraction data.

The pressure dependence of the reflection intensity was investigated. No remarkable change of the intensity was detected for reflections which were observed under all pressure conditions in case of $F>3\sigma(F)$ (F and $\sigma(F)$ denote the observed structure factor and its deviation, respectively). The sum of the observed structure factors for such reflections under each pressure is shown in Fig.2-3-6 (No reflections were observed under 6.5 and 7.3 GPa. Therefore, the structure factors under 6.5 and 7.3 GPa were treated as 0, respectively).

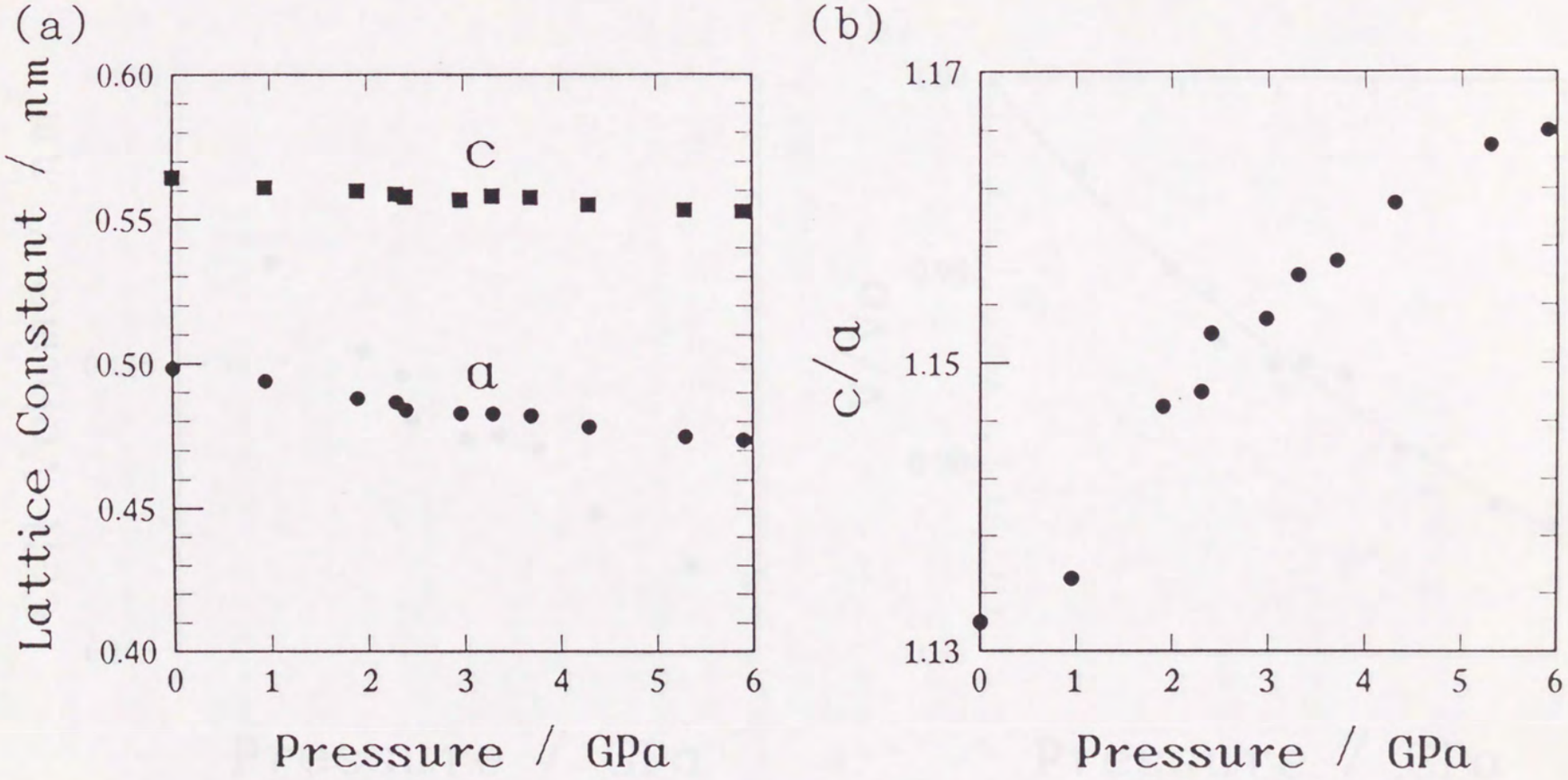

Fig.2-3-4(a),(b) (a) Pressure dependence of lattice constants. (b) Change of c/a ratio with increasing pressure.

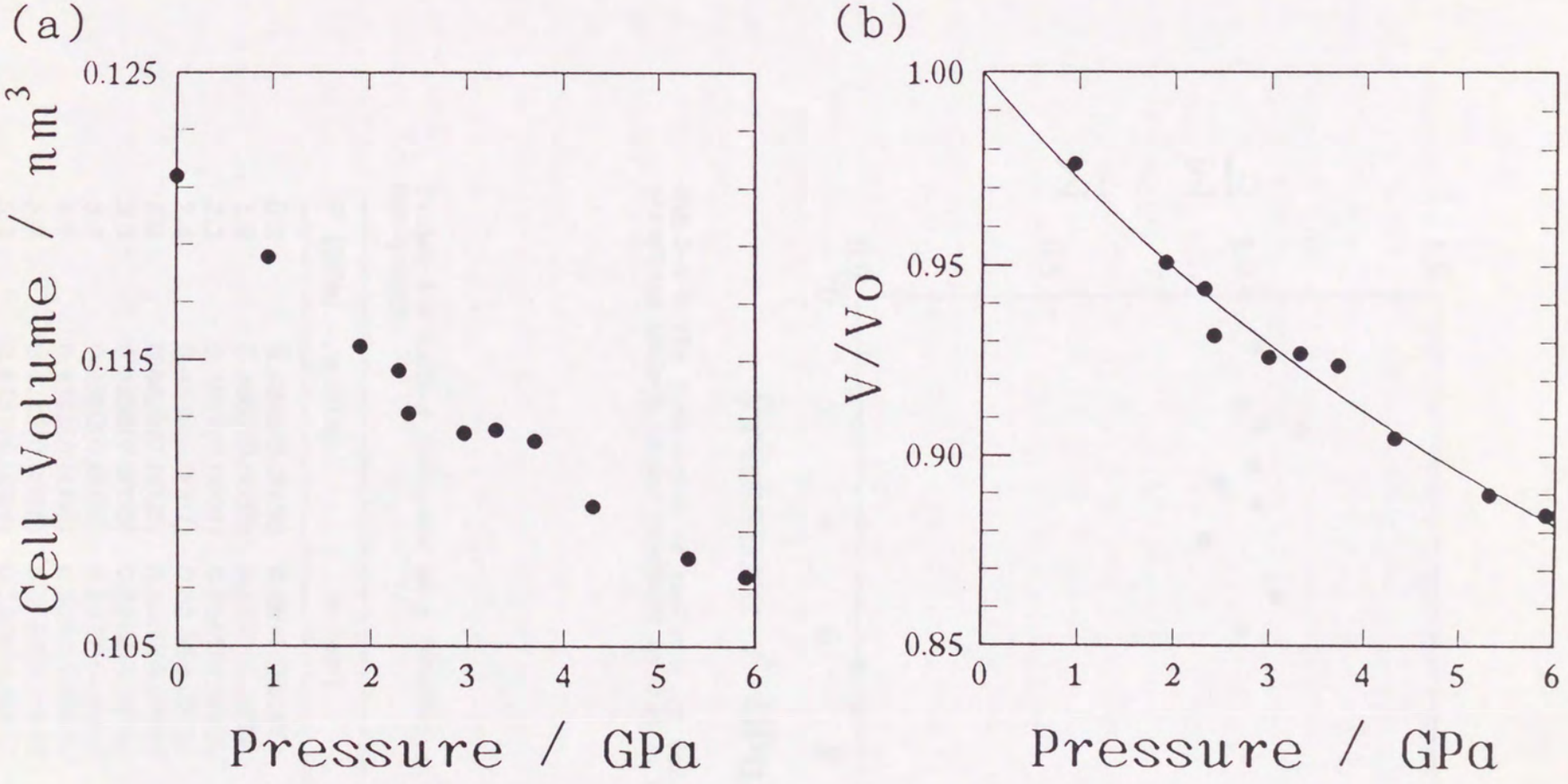

Fig.2-3-5(a),(b) (a) Pressure dependence of unit cell volume. (b) Change of V/Vo ratio with increasing pressure. Solid curve is fitted to the Birch-Murnaghan's equation of state.

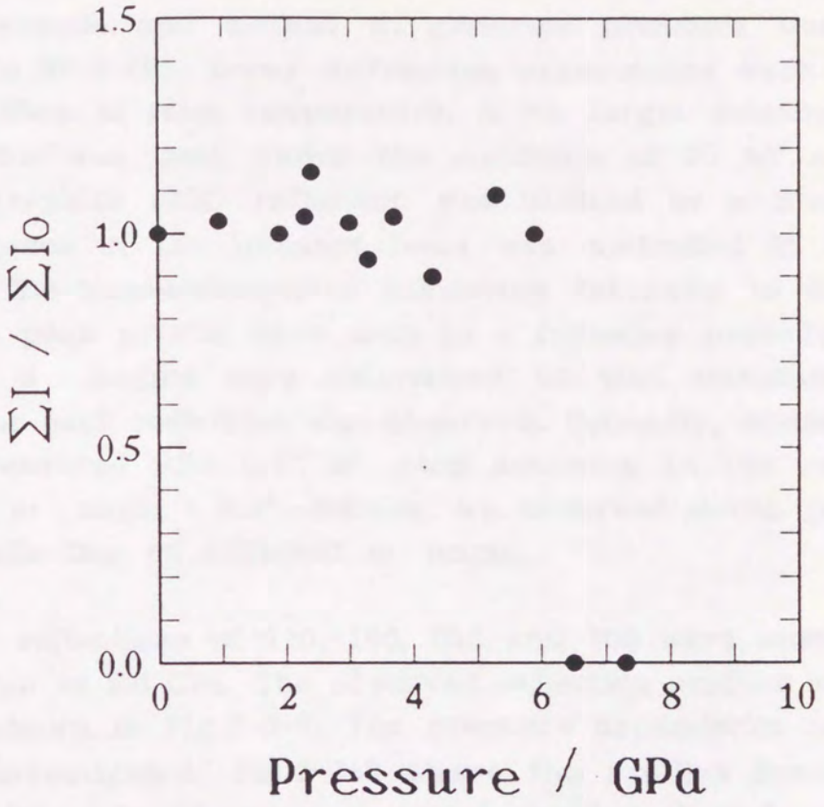

Fig.2-3-6 The proportion of the sum of the observed structure factors under pressure to that at 1 atm.

Table2-3-1 Lattice constants as a function of pressure for q-GeO_2

P (GPa)	a (nm)	c (nm)
0.9	0.4940(0.0003)	0.5611(0.0006)
1.9	0.4880(0.0002)	0.5600(0.0004)
2.3	0.4867(0.0002)	0.5589(0.0003)
2.4	0.4840(0.0007)	0.5578(0.0011)
3.0	0.4829(0.0002)	0.5569(0.0004)
3.3	0.4826(0.0003)	0.5582(0.0004)
3.7	0.4820(0.0002)	0.5577(0.0004)
4.3	0.4781(0.0004)	0.5551(0.0006)
5.3	0.4749(0.0001)	0.5533(0.0003)
5.9	0.4737(0.0004)	0.5528(0.0018)

C) Single-crystal X-ray Diffraction Measurement of α-quartz type GeO_2 under Pressure II

(1) Experimental Details

The sample and method to generate pressure were same as mentioned in §2-3-(B). X-ray diffraction experiments were carried out with PF system at room temperature. A Mo target rotating anode X-ray generator was used under the condition of 50 kV and 100 mA. Pyrolytic graphite (002) reflection was utilized as a monochrometor. The divergence of the incident beam was controlled in a 0.8 mmϕ collimator. The measurements of scattering intensity to get a three-dimensional peak profile were done in a following procedure. Firstly, the ω, χ, ϕ angles were determined so that maximum scattering intensity for each reflection was observed. Secondly, scattering intensity was measured with 0.1° ω step scanning in the range of the determined ω angle ± 0.3°. Namely, we observed seven peak profiles for each reflection on different ω angle.

(2) Results

Four reflections of 110, 103, 013 and 105 were observed under pressures up to 5.6 GPa. The observed reflection profiles with ω rotation were shown in Fig.2-3-7. The pressure dependence of peak profiles was investigated. Fig.2-3-8 shows the profiles having maximum scattering intensity of seven observed profiles at each pressure. No remarkable change as a function of pressure was observed, although the peak position shifted toward higher 2θ angle side as increasing pressure.

The seven observed profiles for one reflection on different ω angle provided a three-dimensional profile as schematically shown in Fig.2-3-9. We also investigated the change of the three-dimensional profiles on compression. As shown in Fig.2-3-9, the profiles did not change remarkably up to 5.6 GPa. Judging from the experimental results mentioned above, no noticeable disorder of crystal symmetry occurred at least up to 5.6 GPa.

It was reported by Hazen et al.[43] that the diffraction line of α-quartz (SiO_2) broadened at about 15 GPa which was almost 10 GPa below its amorphization pressure. Our result on q-GeO_2 is inconsistent with the report on SiO_2.

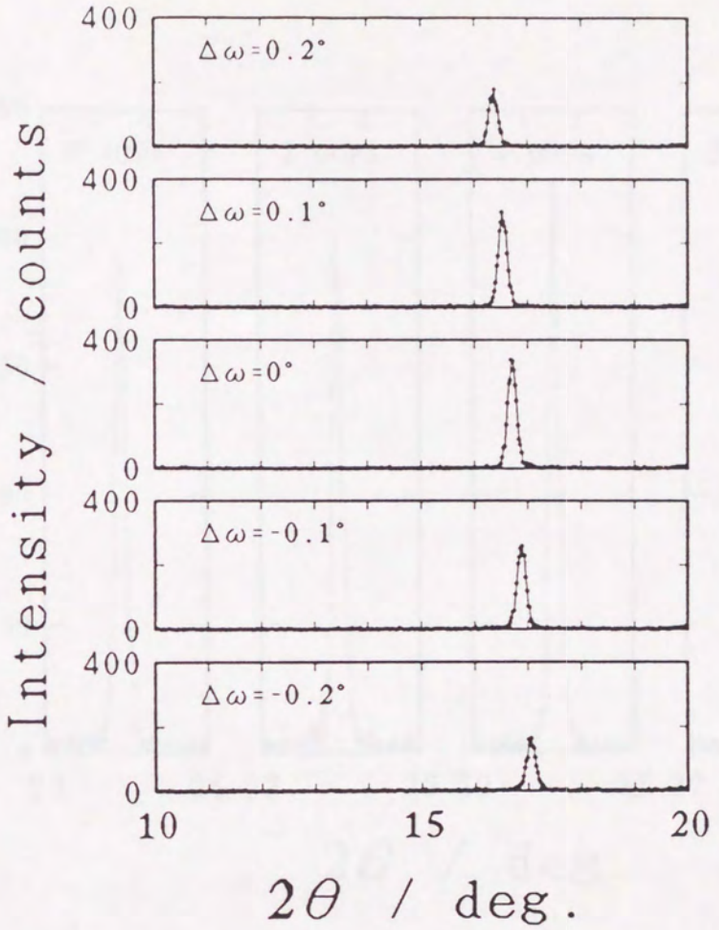

Fig.2-3-7 Change of the observed profile (110 reflection at 0.4 GPa) with ω rotation. Each spectrum was observed for the duration of 20 seconds. Mo Kα irradiated.

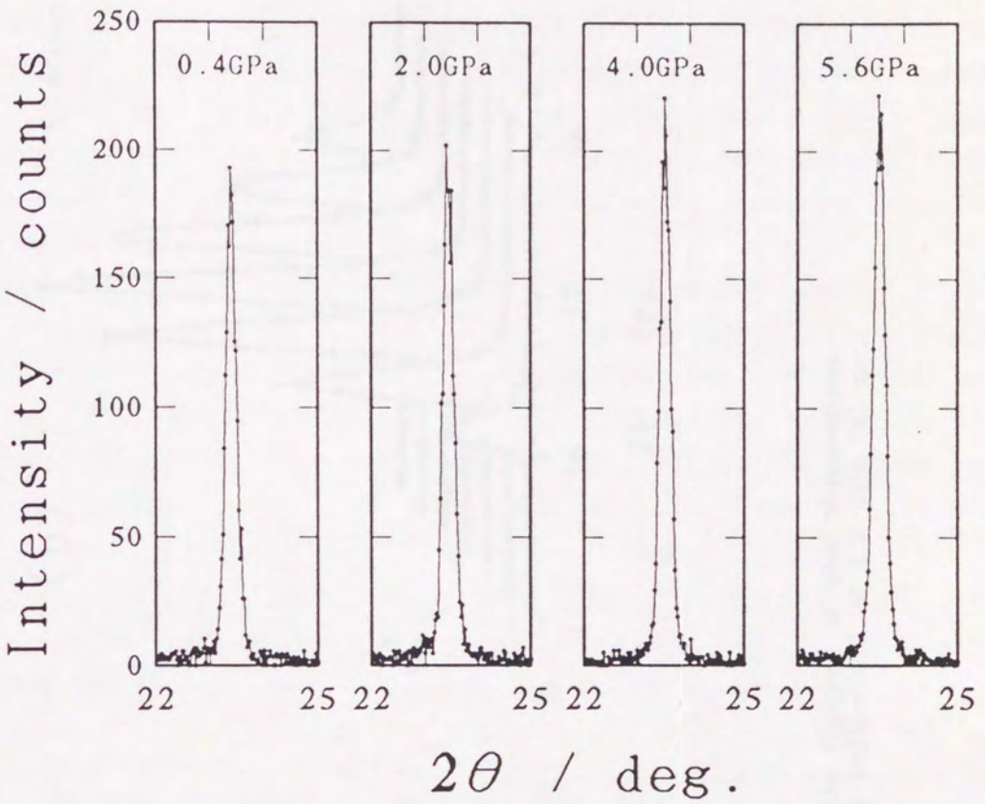

Fig.2-3-8 Pressure dependence of the observed reflection profile (103 reflection). Each spectrum was observed for the duration of 20 seconds. Mo Kα irradiated.

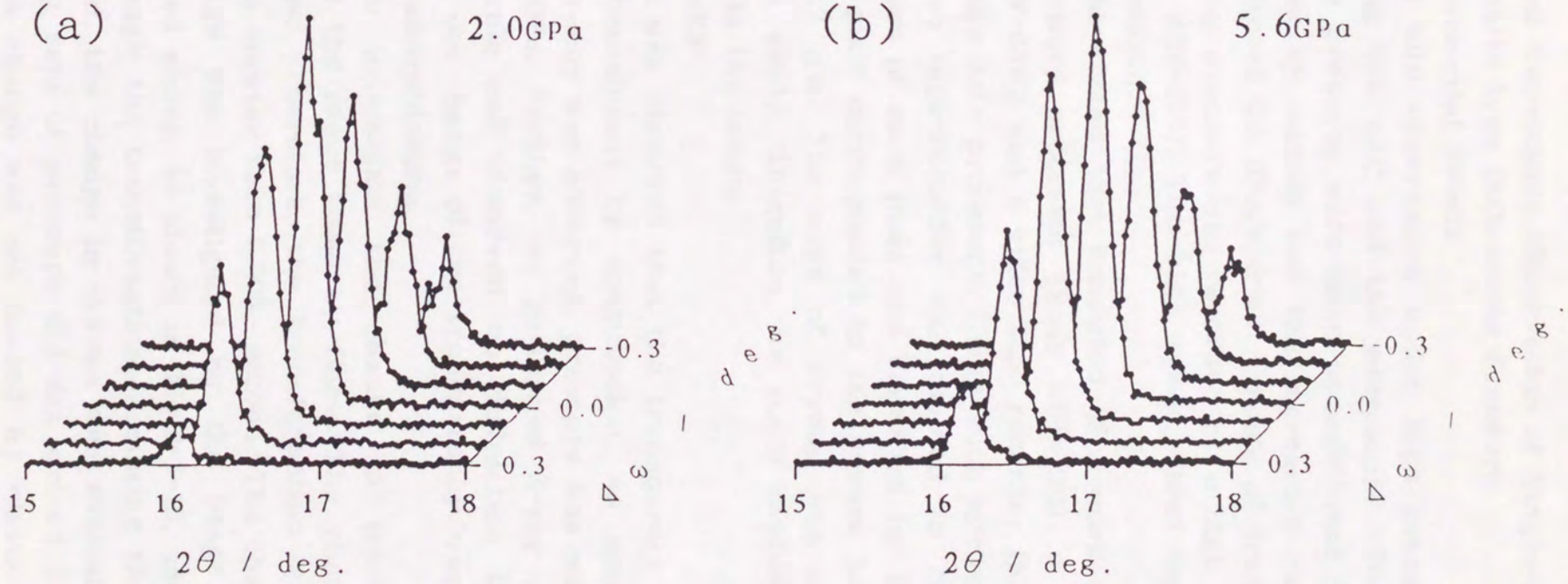

Fig.2-3-9(a),(b) Schematic figures of the three-dimensional peak profile (110 reflection) at 2.0 GPa (a) and 5.6 GPa (b).

D) Optical Microscopic Observation of Single-Crystal
α-quartz type GeO_2 under Pressure

(1) Experimental Details

In situ observation under high pressure was carried out by combining the DAC and the microscope. The sample and method to generate pressure were same as mentioned in §2-3-(B). Pressure was controlled by manual and the increasing rate of pressure was kept not to exceed 0.1 GPa/second. Change of transmitting light image with increasing pressure was recorded by a high speed video tape-recorder (Nac HSV-200). The high speed video tape-recorder recorded 200 flames/second.

The system that consisted of a work station (Sony NWS-831), a flame memory processor (Sony NWB-224), a time base corrector (National AV-6350) and a video tape recorder (National NV-8950) was used as a image data processor. Using such system, the image recorded by the video tape-recorder was divided to 768 x 480 pixels and the brightness of each pixel was classified by 256 grade. In this experiment, 1 pixel corresponded to the square having dimensions of about 0.7 x 0.7 μm. The edge of crystal was apparently dark and was detected easily. Therefore, we could evaluate the occupied area by crystal in the image.

(2) Results

It was observed that the transparent crystal abruptly changed to be translucent by compression. As soon as the change of the transparency was observed, pressure was measured and determined to be 6.5 GPa. Further, we performed X-ray diffraction experiment for the sample and observed no diffraction line. Judging from these results, the change of the transparency was considered to be caused by the amorphization.

To investigate the change in transparency with time, we checked the image flame by flame. The change was completed within one flame. Therefore, the transformation was completed within time duration shorter than 0.005 second. The change of the sample area in the image was investigated by the image data processing system mentioned above. As shown in Fig.2-3-10, the area was shrunk by 5-7% through the transformation. Assuming that an isotropic shrinkage occurred, the change in volume was evaluated to be 7-11%. The increasing rate of pressure did not exceed 0.1 GPa/second. Therefore, the area change was not caused by elastic deformation, but by the transformation. Further, the area of the translucent material did not change markedly in 0.15 second from the onset of the transition (Fig.2-3-10). Namely, the amorphization completed within time duration

shorter than 0.005 second. From this time forward, we treat the observed translucent material as high pressure amorphous GeO_2. For convenience sake, the observed translucent material is abbreviated to a-GeO_2(OM).

The change in transparency with the amorphization was considered to be explained as follows. The amorphization took place with volume change of 7-11 % mentioned above. If nucleation occurred in several places of the single-crystal, shear stresses in the transformed area were caused by the volume change. Single-crystal had to be polycrystallized for the relaxation of the shear stresses. For all of surface induced by the polycrystallization, reflection of the sample was increased. Therefore, the transparency of the sample was decreased.

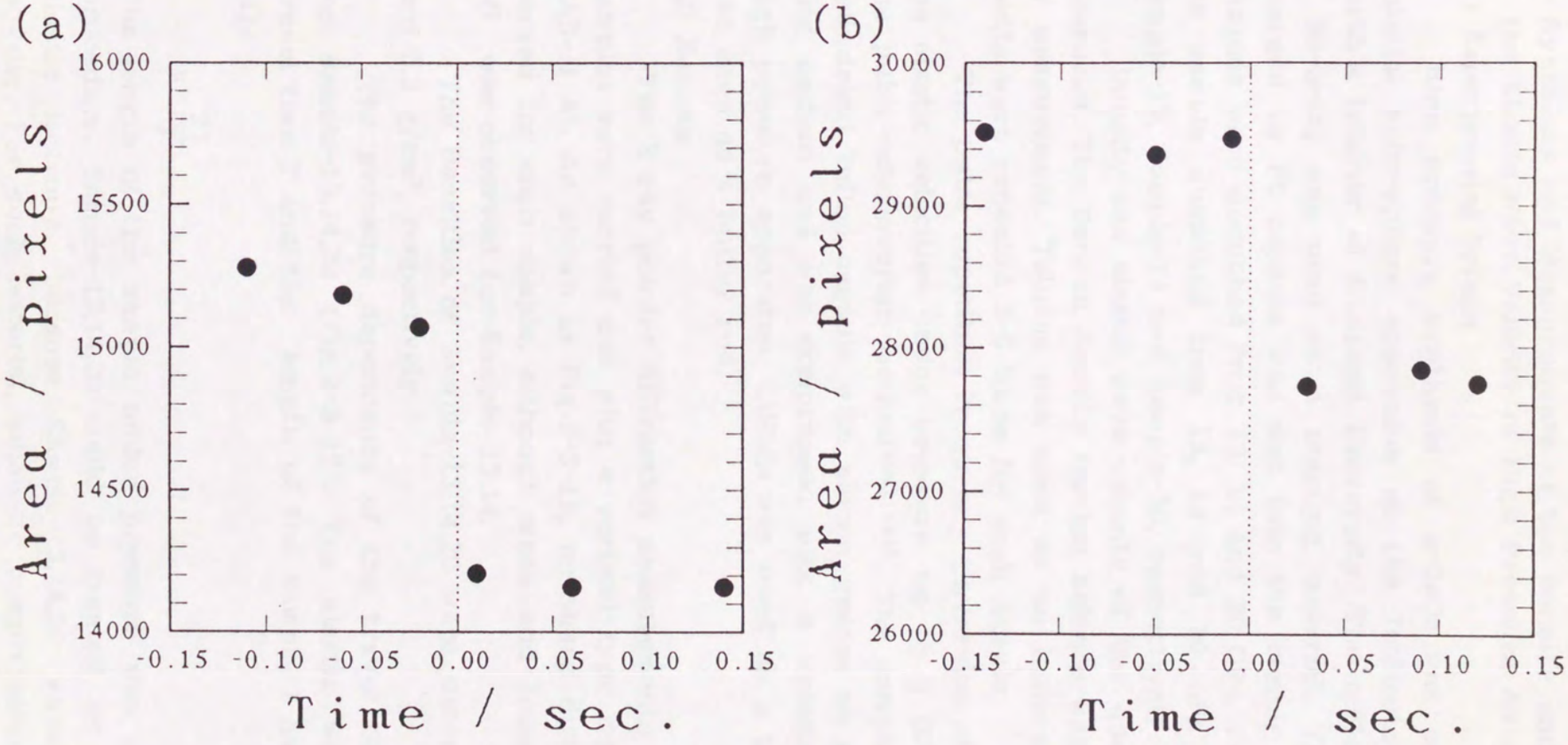

Fig.2-3-10(a),(b) Change of the observed sample area with time for small(a) and large(b) sample. The origin of time was set at when the change of the transparency was brought about.

E) Synthesis and Measurements of the Density and the Elastic Wave Velocity of High Pressure Amorphous GeO_2

(1) Experimental Details

High pressure synthesis of a-GeO_2 was carried out using a uniaxial split-sphere apparatus at the Institute for Study of the Earth's Interior of Okayama University. The q-GeO_2 sample mentioned in §2-3-(A) was used as a starting material. The starting material charged in Pt capsule was put into the center of MgO octahedron. Samples were quenched from 13, 14 and 20 GPa. For convenience sake, the sample quenched from 13, 14 and 20 GPa are abbreviated to Sample-13, Sample-14 and Sample-20, respectively.

Density and elastic wave velocity of the quenched samples were measured. The Berman density torsion balance was used for the density measurement. Toluene was used as an immersion liquid. Measurements were repeated 3-5 times for each sample.

The pulse-repetition frequency (inversion of the travel time) for the elastic velocities under pressure up to 3 GPa was measured by the pulse-echo-overlap method[44],[45]. The sample was inserted in a cylindrical Teflon capsule with silicon grease as a pressure transmitting medium and was compressed with a uniaxial split-sphere type high pressure apparatus. $LiNbO_3$ was used as a transducer and CuZn was used as a buffer rod.

(2) Results

The X-ray powder diffraction measurements for the all quenched samples were carried out with a vertical type diffractometer (RIGAKU RAD-II A). As shown in Fig.2-3-11, no sharp diffraction line was observed for each sample, although weak and broad peak near 26° in 2θ was observed for Sample-13,14.

The densities of Sample-13,14,20 were determined to be 4.4, 4.8 and 5.3 g/cm^3, respectively.

The pressure dependence of the travel time was investigated for Sample-13,14,20 (Fig.2-3-12). The elastic wave velocity v, the travel time T and the length of the sample l have following relation (1).

$$v = \frac{2l}{T} \tag{1}$$

The length of the sample under pressure was obtained as following procedure. Sample-13,14,20 could be treated as the material having elastic isotropy, because Sample-13,14,20 were the aggregate of powder. For such material, adiabatic compressibility κ_s, elastic wave velocity can be represented by relation (2).

$$\frac{1}{\kappa_s} = \rho \left(v_p^2 - \frac{4}{3} v_s^2 \right) \quad (2)$$

where ρ is the density, v_p is the longitudinal wave velocity, v_s is the shear wave velocity.

The isothermal compressibility κ_t is calculated by relation(3).

$$\kappa_t = \kappa_s + \frac{\alpha^2 T}{\rho C_p} \quad (3)$$

where α is the thermal expansion coefficient, T is temperature, Cp is the heat capacities at constant pressure.

Since α and Cp were unknown for Sample-13,14,20 and in general the difference between κ_t and κ_s is within a few percents, here κ_t is approximated by κ_s.

$$\kappa_t \fallingdotseq \kappa_s \quad (4)$$

In accordance with a small increment of pressure ΔP, an increment of volume ΔV is expressed by following relation (5).

$$\frac{\Delta V}{V} = \kappa_t \Delta P \quad (5)$$

where V and κ_t is the volume and the isothermal compressibility at P. For the elastic isotropic material, the length of the sample at P and P+ΔP are expressed by following relation (6).

$$\frac{l'}{l} = \left(1 - \frac{\Delta V}{V} \right)^{\frac{1}{3}} \quad (6)$$

where l and l' is the length at P and P+ΔP.

The travel time at P+ΔP is obtained by fitting a series of experimental data to the following polynomial relation (7).

$$T(P) = a_0 + a_1 P + a_2 P^2 + \cdots\cdots \quad (7)$$

where T(P) is the travel time at P, a_i(i=0,1,2...) are constants.

The ultrasonic wave velocity v' at P+ΔP was obtained with l' in relation (6) and T(P+ΔP) in relation (7).

$$v' = \frac{2l'}{T(P+\Delta P)} \quad (8)$$

The volume V' at P+ΔP is expressed by following relation (9).

$$\frac{V'}{V} = 1 - \kappa_t \Delta P \quad (9)$$

The pressure dependencies of the elastic wave velocity and of the volume were obtained (Fig.2-3-13,14) by repeating the sequence of the procedure. The isothermal bulk modulus Kt and its pressure derivative Kt' were obtained by fitting V/Vo to the Birch-Murnaghan's equation of state. Kt and Kt' for Sample-13,14,20 were determined to be 52.2(0.3), 60.4(0.4), 76.6(0.9) GPa and 7.6(0.4), 7.4(0.4), 9.6(1.0).

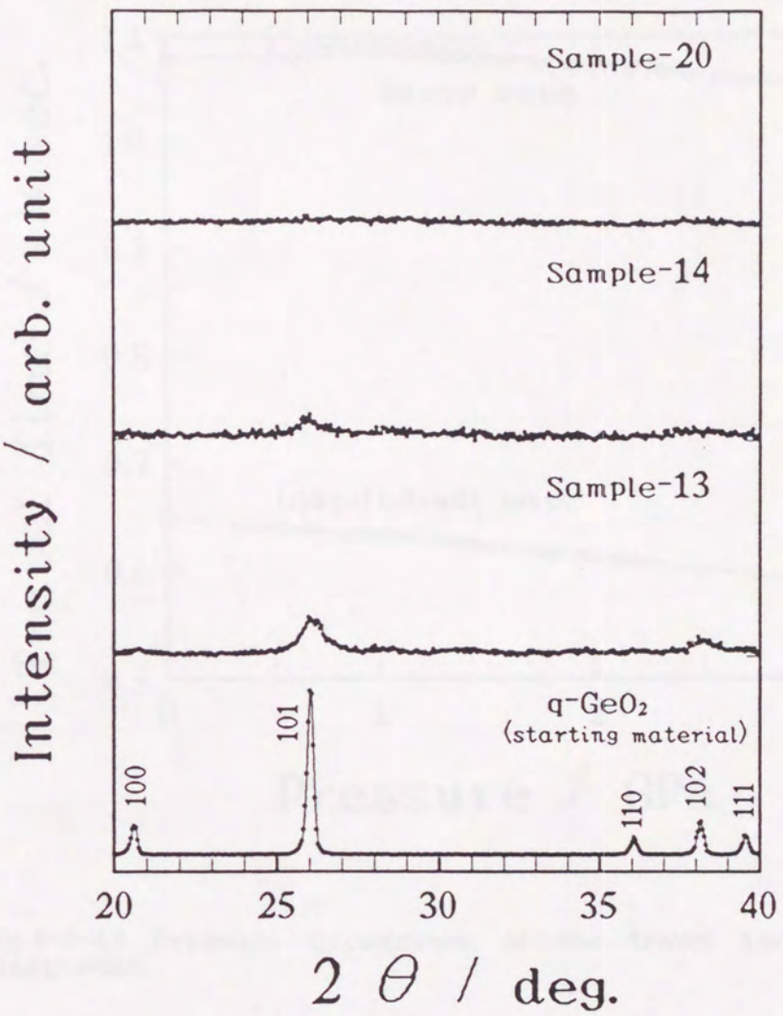

Fig.2-3-11 Observed diffraction patterns of Sample-13,14,20 and of q-GeO_2. Cu Kα irradiated.

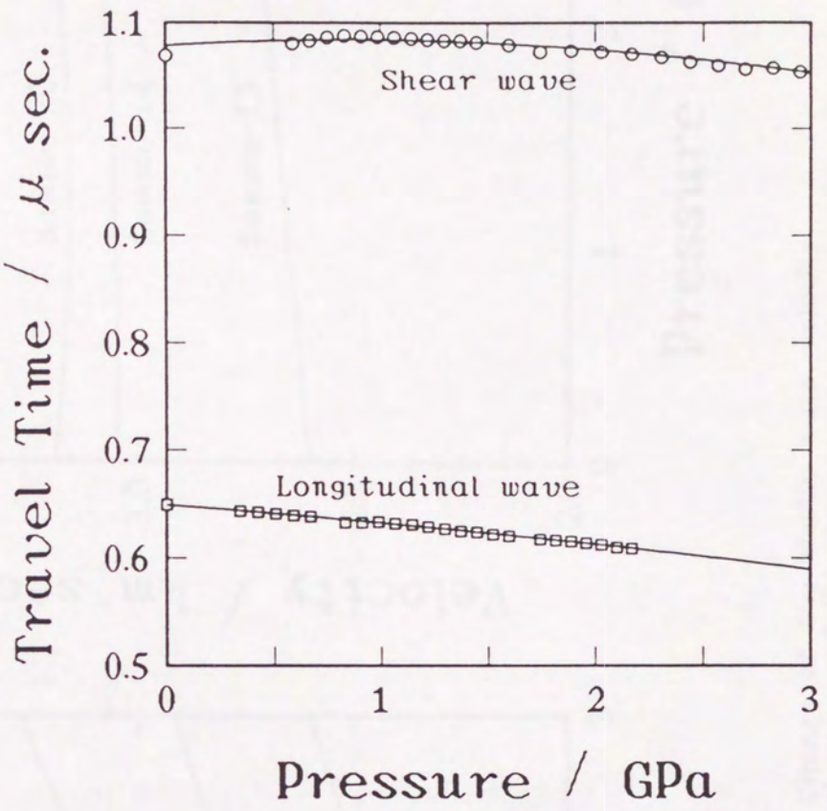

Fig.2-3-12 Pressure dependence of the travel time (Sample-20).

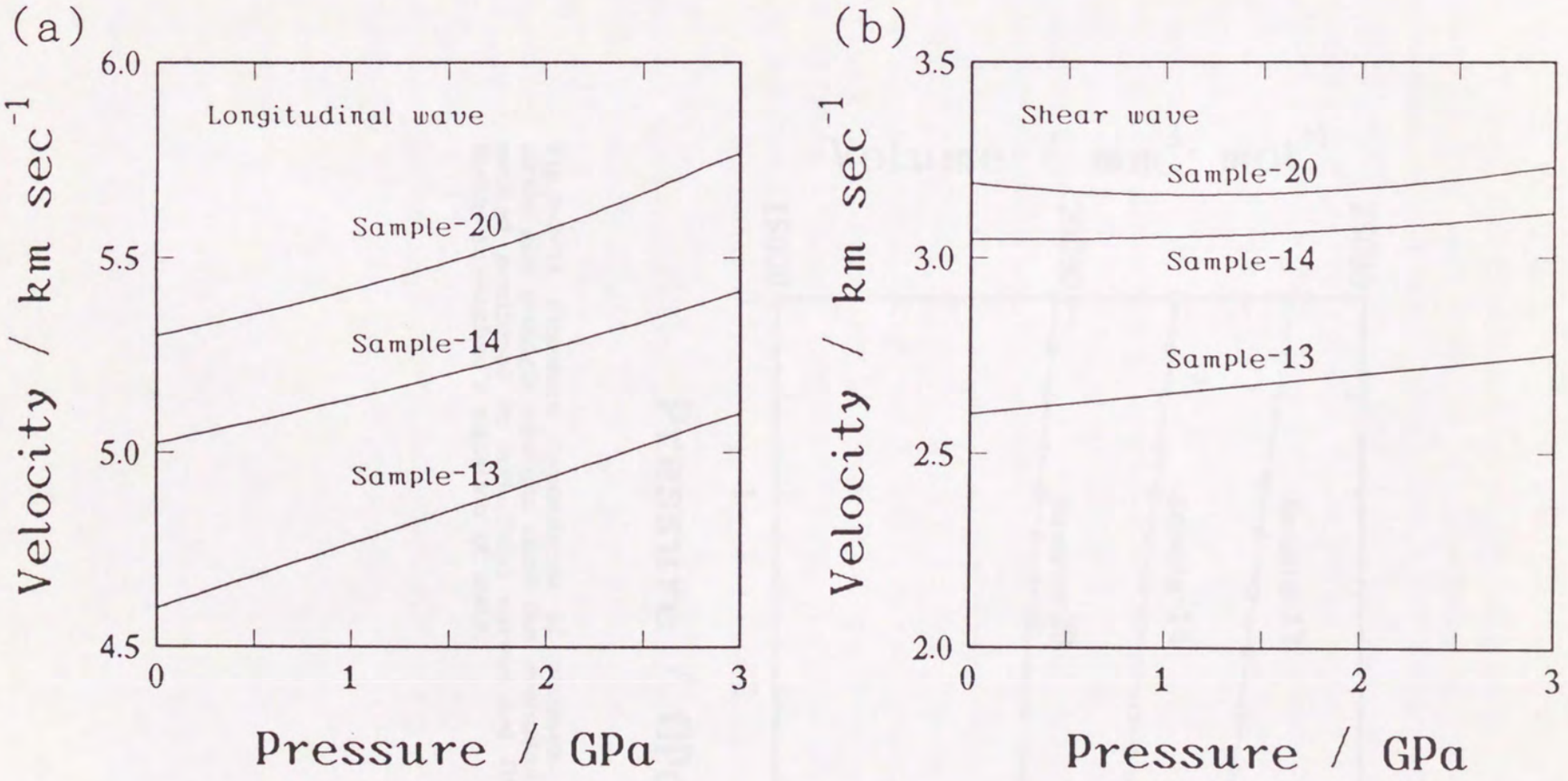

Fig.2-3-13(a),(b) Change of the elastic wave velocity for (a) longitudinal wave and (b) shear wave.

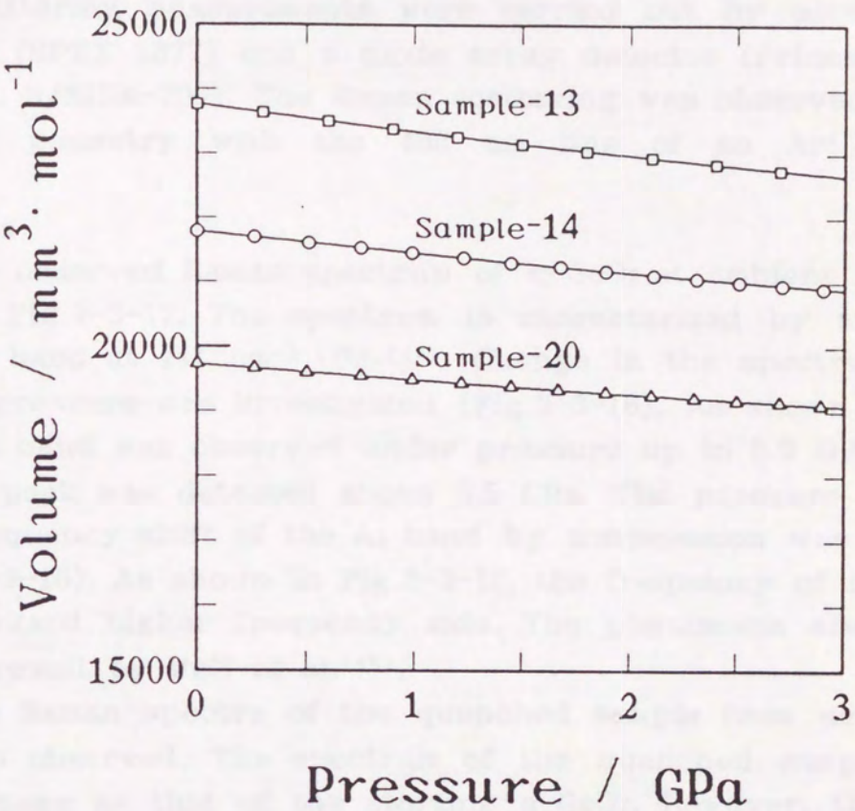

Fig.2-3-14 Pressure dependence of volumes. Square, circle and triangle symbols show the evaluated by the method mentioned in text. Solid curves are fit to the Birch-Murnaghan's equation of state.

F) Raman Scattering Experiment

(1) Experimental Details

In situ Raman scattering experiment under high pressure was performed. The sample and DAC were same as mentioned in §2-3-(A). The mixture of methanol : ethanol = 4 : 1 was used as a PTM. Micro-Raman scattering measurements were carried out by using an polychrometor (SPEX 1877) and a diode array detector (Princeton Instruments Inc. h/SIDA-700). The Raman scattering was observed in a back scattering geometry with the 488 nm line of an Ar^+ laser (NEC GLG3300).

(2) Results

The observed Raman spectrum of q-GeO_2 at ambient pressure is shown in Fig.2-3-15. The spectrum is characterized by an extremely strong A_1 band at 441 cm^{-1} [46],[47]. Change in the spectrum with increasing pressure was investigated (Fig.2-3-16). As shown in Fig.2-3-16, the A_1 band was observed under pressure up to 6.0 GPa. However, no sharp peak was detected above 6.5 GPa. The pressure dependence of the frequency shift of the A_1 band by compression was investigated (Fig.2-3-16). As shown in Fig.2-3-16, the frequency of the A_1 band shifted toward higher frequency side. The phenomena are consistent with the result by Wolf et al.[48].

The Raman spectra of the quenched sample from several pressure were observed. The spectrum of the quenched sample from 6.0 GPa was same as that of the starting q-GeO_2. However, the spectrum of the quenched sample from 12 GPa was different from that of the starting (Fig.2-3-17). We could observe 3 bands marked in this Fig.2-3-17, although each peak was weak and broad. Two bands near 400 and 700 cm^{-1} was considered to correspond to the observed bands of the quenched sample from 20 GPa by Wolf et al.[48] (They assigned the band at 700 cm^{-1} as A_{1g} of r-GeO_2). The band near 450 cm^{-1} was considered to be the A_1 band of q-GeO_2.

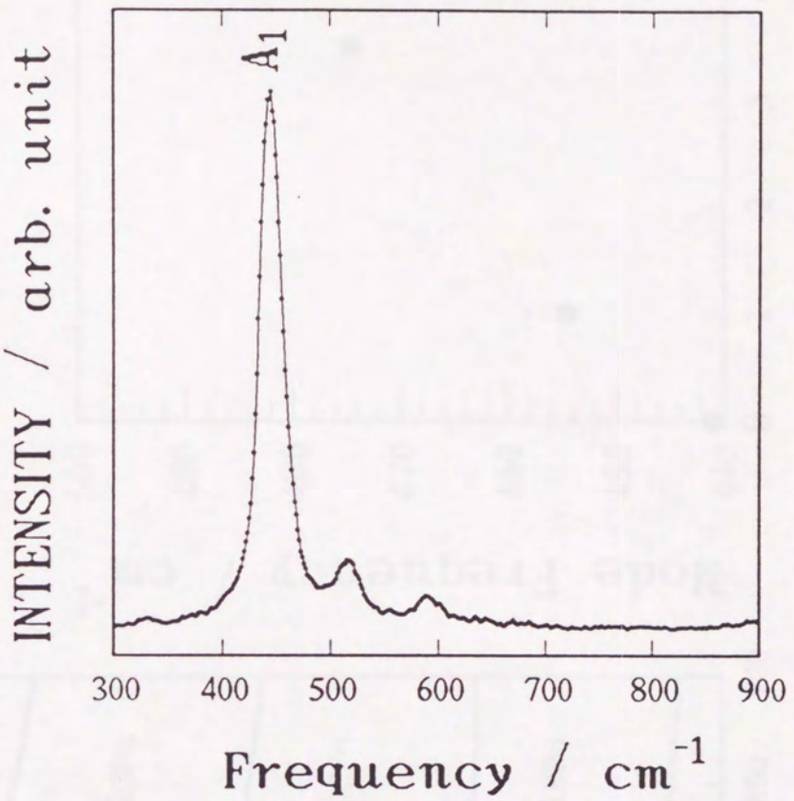

Fig.2-3-15 Observed Raman scattering spectrum of q-GeO_2 under room condition.

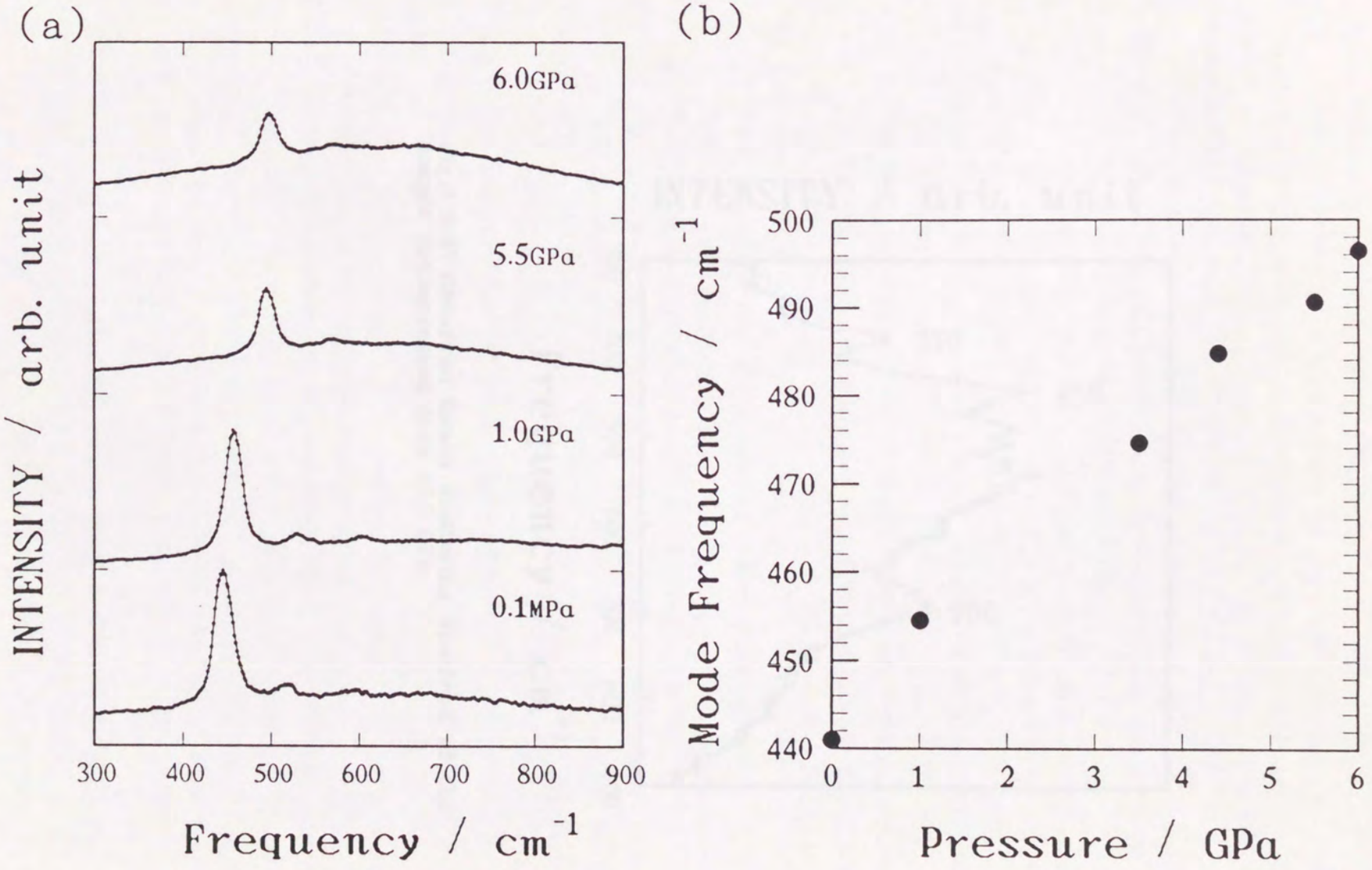

Fig.2-3-16(a),(b) (a) Change of the Raman scattering spectrum with increasing pressure. (b) Change of the peak frequency of A_1 mode with increasing pressure.

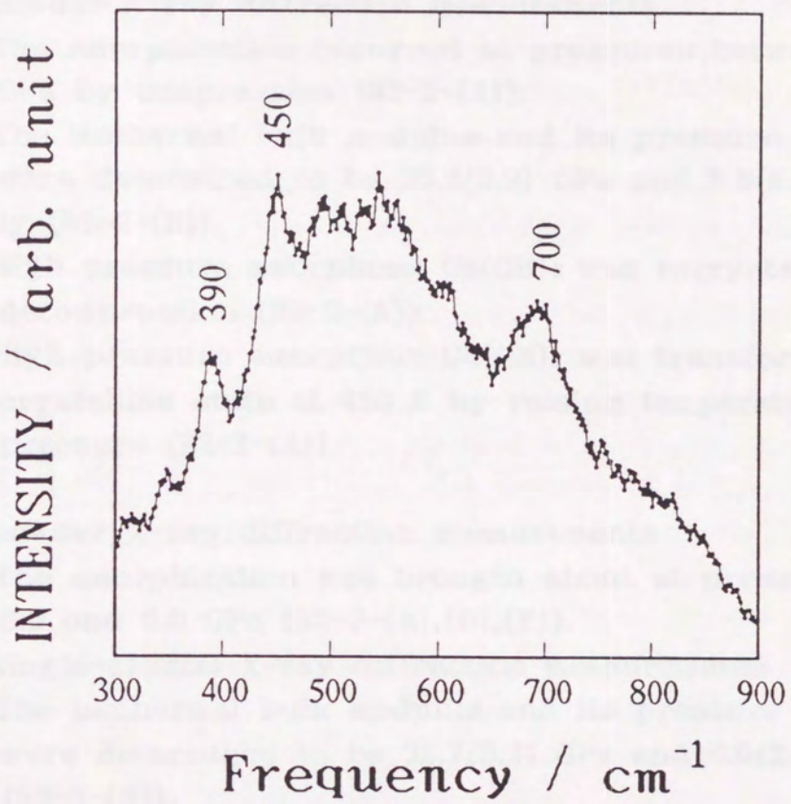

Fig.2-3-17 Observed Raman scattering spectrum of the sample decompressed from 12.0 GPa.

§2-4 Summary of Experimental Results

We performed several experiments to investigate the pressure induced amorphization of $Ca(OH)_2$ and q-GeO_2. The results are summarized as follows.

A) $Ca(OH)_2$

By powder X-ray diffraction measurements

(1) The amorphization occurred at pressures between 10 and 12 GPa by compression (§2-2-(A)).

(2) The isothermal bulk modulus and its pressure derivative were determined to be 30.4(2.9) GPa and 8.6(1.8), respectively (§2-2-(B)).

(3) High pressure amorphous $Ca(OH)_2$ was recrystallized on decompression (§2-2-(A)).

(4) High pressure amorphous $Ca(OH)_2$ was transformed to a crystalline state at 450 K by raising temperature under pressure (§2-2-(A)).

B) q-GeO_2

By powder X-ray diffraction measurements

(1) The amorphization was brought about at pressures between 6.0 and 8.0 GPa (§2-3-(A),(B),(F)).

By single-crystal X-ray diffraction measurements

(2) The isothermal bulk modulus and its pressure derivative were determined to be 32.7(3.3) GPa and 6.0(2.2),respectively (§2-3-(B)).

By optical microscope observations

(3) The volume change by the amorphization was evaluated to be 7-11 % (§2-3-(B)).

C) a-GeO_2

By powder X-ray diffraction measurements

(1) a-GeO_2 was not transformed to q-GeO_2 on decompression to 0.1 MPa in the most experimental conditions (§2-3-(A)).

By density measurements

(2) The density of Sample-13,14,20 was 4.4, 4.8 and 5.3 g/cm^3, respectively (§2-3-(E)).

By elastic wave velocity measurements

(3) The isothermal bulk modulus and its pressure derivative of Sample-13,14,20 were evaluated to be 52.2(0.3), 60.4(0.4), 76.6(0.9) GPa and 7.6(0.4), 7.4(0.4), 9.6(1.0) (§2-3-(E)).

By Raman scattering measurements

(4) The band at 700 cm^{-1} was observed in the spectrum of the sample quenched from 12 GPa. It may be assigned as A_{1g} mode of r-GeO_2 (§2-3-(F)).

§3 Discussions

§3-1 Pressure Induced Amorphization of $Ca(OH)_2$

(A) Driving Force of the Amorphization

A transformation under high pressure is often caused by shear stress[49],[50]. The experiments under hydrostatic and non-hydrostatic pressure were performed to investigate the effect of shear stress on the amorphization of $Ca(OH)_2$. It was shown that no remarkable difference by hydrostaticity was detected in the observed X-ray powder diffraction patterns. Further, in the amorphization of $Ca(OH)_2$, reverse transition from the amorphous to the crystalline phase took place. As mentioned above, the transition is caused by changes in pressure.

(B) Mechanism of the Amorphization

There are two important reports on the mechanism of the amorphization of $Ca(OH)_2$. Firstly, Kruger et al.[8] performed infrared spectroscopy experiments to pressures of 24 GPa. They reported that the O-H vibrational peak width increased abruptly by 300 cm^{-1} at 11.7 GPa. Secondly, Meade et al.[51] carried out in situ Raman observations under pressure up to 20.1 GPa. It was observed that a new peak at 3639 cm^{-1} appeared at 10.8 GPa.

We performed in situ X-ray observations under high pressure and observed that there was a discontinuous loss in the diffracted X-ray intensity between 10 and 12 GPa. We consider that the amorphization occurred drastically between 10 and 12 GPa by following reasons. Firstly, the 101 diffraction line was sharp just before the transition to the amorphous state. Therefore, the sample existed as crystalline state up to 10 GPa. Secondly, the new Raman band that was observed by Meade et al.[51] was not detected at 9.8 GPa. Thirdly, the line broadening of infrared spectra that was observed by Kruger et al.[8] took place at pressures between 10.6 and 11.7 GPa.

As mentioned above, the amorphization of $Ca(OH)_2$ is considered to occur at about 11 GPa and complete within 2 GPa. Further, the activation energy for the amorphization was considered to be small, because the transition occurred drastically at ambient temperature without heating. Therefore, the amorphization is considered to be displasive transition without diffusion process.

§3-2 Pressure Induced Amorphization of GeO_2

(A) Equations of States of GeO_2 Polymorphs

We discuss the amorphization of q-GeO_2 with the information on the equations of states of GeO_2 polymorphs. Molar volume is one of the most important variables from the thermodynamical point of view. We should know molar volumes of the starting and transformed phases to discuss their phase relation.

Here, we use the Birch-Murnaghan's equation of state (see §2-2-(B)).

(1) q-GeO_2, r-GeO_2

We determined that the isothermal bulk modulus K_t and its pressure derivative K_t' of q-GeO_2 was 32.7(3.3) GPa and 6.0(2.2), respectively (§2-3-(B)). For r-GeO_2, we adopt K_t=265(4) and K_t'=4 (assumed) that were determined by Hazen et al.[52] The pressure dependencies of q-GeO_2 and r-GeO_2 are shown in Fig.3-2-1.

(2) a-GeO_2

[I] a-GeO_2(OM)

The volume change of the sample with the amorphization was evaluated as 7-11 %. The transition pressure was determined to be 6.5(0.5) GPa (§2-3-(D)). The solid square labeled OM in Fig.3-2-1 shows a-GeO_2(OM).

[II] Sample-13,14,20

The densities of the quenched sample from 13, 14 and 20 GPa (Sample-13,14,20) were determined to be 4.4, 4.8 and 5.3 g/cm^3, respectively (§2-3-(E)). Therefore, the molar volumes of Sample-13,14,20 under room condition were evaluated as illustrated by solid square labeled a1,a2,a3 in Fig.3-2-1. As mentioned in §2-3-(D), the isothermal bulk modulus K_t and its pressure derivative K_t' of Sample-13,14,20 were determined to be 52.2(0.3), 60.4(0.4), 76.6(0.9) GPa and 7.6(0.3), 7.4(0.4), 9.6(1.0) for Sample-13,14,20, respectively. The pressure dependencies of their volumes were shown with line-A1,A2,A3 in Fig.3-2-1.

The solid square labeled OM in Fig.3-2-1 must be on one of the line-A1, A2 and A3, if a-GeO_2(OM) was quenchable. However, the solid square labeled OM is not on any line. Therefore, a-GeO_2(OM) is considered to be unquenchable.

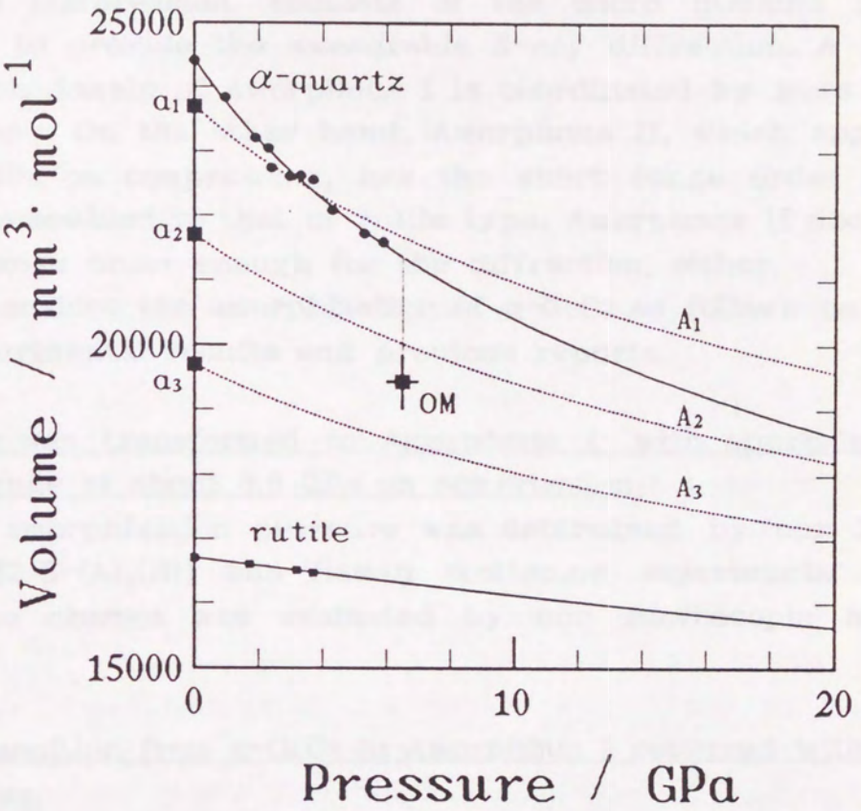

Fig.3-2-1 Equation of state data for GeO_2 polymorphs.

(B) Two Amorphous States Model

The behavior of GeO_2 under high pressure could be explained with the model of the presence of two high pressure amorphous states (Amorphous I,II). Amorphous I, which appears from about 6.5 to about 11 GPa on compression, consists of the micro domains lacking of dimensions to provide the measurable X-ray diffraction. A germanium atom in each domain of Amorphous I is coordinated by more than four oxygen atoms. On the other hand, Amorphous II, which appears from about 11 GPa on compression, has the short range order of crystal symmetry resembled to that of rutile type. Amorphous II does not have the long range order enough for the diffraction, either.

We consider the amorphization of q-GeO_2 as follows on the basis of our experimental results and previous reports.

(1) q-GeO_2 was transformed to Amorphous I with approximately 10% volume change at about 6.5 GPa on compression.

The amorphization pressure was determined by our X-ray diffraction (§2-3-(A),(B)) and Raman scattering experiments (§2-3-(E)). The volume change was evaluated by our microscopic observation (§2-3-(D)).

(2) The transition from q-GeO_2 to Amorphous I occurred without diffusion process.

The amorphization occurred at ambient temperature. Therefore, the transition need not large activation energy. Further, the transition completed within time duration shorter than 0.005 second (§2-3-(D)).

It was recently reported by Tsuneyuki et al.[53] that α-quartz (SiO_2) was transformed to an amorphous state without diffusion process by their computer simulation. Since GeO_2 has an analogy of SiO_2, the mechanism of the amorphization of q-GeO_2 is considered to resemble that of α-quartz.

(3) Amorphous I consisted of many domains. A germanium atom was coordinated by more than four oxygen atoms in each domain of Amorphous I.

It was observed by the TEM experiment[48] that the samples quenched from high pressure above 7 GPa were divided to some domains having scale of tens nm.

Since the Ge-O distance increased markedly between 7 and 12 GPa, which was observed by the XANES experiment[9], the coordination number of a germanium atom increased by the amorphization.

(4) The coordination number of a germanium atom in some domains of Amorphous I decreased to approximately four of q-GeO_2 on decompression to ambient pressure.

Since both molar volumes of Sample-13 and 14 at 6.5 GPa were larger than that of a-GeO_2(OM) by the calculation with the obtained equation of state, part of a-GeO_2(OM) made reverse transition. The density of Sample-13 was close to that of q-GeO_2. Further, it was observed by the XANES experiment[9] that the Ge-O length was close to the length in q-GeO_2 on decompression in the case when peak pressure was 9.7 GPa.

(5) Amorphous I was transformed to Amorphous II at pressures between 11 and 20 GPa.

Since the molar volume of Sample-20 at 6.5 GPa was smaller than that of a-GeO_2(OM) by the calculation with the obtained equation of state, the transition from an amorphous to another amorphous state occurred above 6.5 GPa. It was reported[48] that the Raman spectra of the quenched sample from 8.5 GPa and 20 GPa were different and that the pressure dependence of the A_1 mode frequency of q-GeO_2 changed at 7 and 11 GPa. Judging from the report, the transition from an amorphous to another amorphous state might occur at about 11 GPa. On the other hand, we observed that the Raman spectrum of the sample quenched from 12.0 GPa included common bands which were found in Raman spectra of the samples quenched from 8.5 and 20.0 GPa. Therefore, the Amorphous I to Amorphous II transition occurred at 11 GPa, but two amorphous states coexisted in wide pressure range (11-20 GPa).

(6) The structure in the domain of Amorphous II resembled that of r-GeO_2.

The band at about 700 cm^{-1} that was observed in the Raman spectrum of the quenched sample from 12 GPa may be assigned as A_{1g} mode of r-GeO_2 (§2-3-(F)). Further, r-GeO_2 regions was observed in the TEM image of the quenched sample from 20 GPa[48]. As mentioned above, the short range order of Amorphous II resembled that of r-GeO_2. However, since Amorphous II also consisted of small domains having scale of tens nm, we could not observe any X-ray diffraction lines of r-GeO_2.

It is interesting that the high pressure amorphous phase of α-quartz (SiO_2) was transformed to stishovite at about 70 GPa on compression[54].

(7) Amorphous II was quenchable to ambient pressure.

We observed no reflection regardless of pressure transmitting mediums for the quenched sample whose peak pressure was above 20 GPa (§2-3-(A)). Further, the density of Sample-20 was much larger than that of q-GeO_2 (§2-3-(E)).

It was elucidated by XANES experiment[9] that the Ge-O length of the quenched sample from 29.1 GPa elongated from 0.184 nm at 29.1 GPa to 0.187 nm at ambient pressure. A relaxation of GeO_6 octahedra might result the elongation. If reverse transition occurred, the Ge-O length was considered to decrease close to 0.175 nm in q-GeO_2 as seen in the case when peak pressure was 9.7 GPa.

Appendix 1

We give the method to move the reciprocal plane including the reciprocal origin to the detector plane with ϕ and χ rotation. The reciprocal plane including the reciprocal origin is determined by three points (0,0,0), (X_1,Y_1,Z_1) and (X_2,Y_2,Z_2). The coordinate axes and 2θ, ω, χ, ϕ rotation axes are taken as shown in Fig.A-1.

The point (X,Y,Z) moves to the point (X",Y",Z") with ϕ and χ rotation (under the condition ω=0°).

(1) ϕ rotation

$$\begin{pmatrix} X' \\ Y' \\ Z' \end{pmatrix} = \begin{pmatrix} \cos\phi & -\sin\phi & 0 \\ \sin\phi & \cos\phi & 0 \\ 0 & 0 & 1 \end{pmatrix} \begin{pmatrix} X \\ Y \\ Z \end{pmatrix}$$

(2) χ rotation

$$\begin{pmatrix} X'' \\ Y'' \\ Z'' \end{pmatrix} = \begin{pmatrix} \cos\chi & 0 & \sin\chi \\ 0 & 1 & 0 \\ -\sin\chi & 0 & \cos\chi \end{pmatrix} \begin{pmatrix} X' \\ Y' \\ Z' \end{pmatrix}$$

The purpose is to make both Z_1" and Z_2" be zero ((X_1,Y_1,Z_1) and (X_2,Y_2,Z_2) moves to (X_1",Y_1",Z_1") and (X_2",Y_2",Z_2") with ϕ and χ rotation). Therefore, we get a following simultaneous equation.

$$Z_1\cos\chi - X_1\sin\chi\cos\phi + Y_1\sin\chi\sin\phi = 0$$
$$Z_2\cos\chi - X_2\sin\chi\cos\phi + Y_2\sin\chi\sin\phi = 0$$

The required ϕ and χ angles are given as follows by resolving the simultaneous equation.

$$a = \pm\frac{|X_1Z_2 - X_2Z_1|}{\sqrt{(X_1Z_2 - X_2Z_1)^2 + (Y_1Z_2 - Y_2Z_1)^2}}$$

$$b = \pm\frac{|Z_1|}{\sqrt{Z_1^2 + (X_1\sqrt{1-a^2} - Y_1a)^2}}$$

$$a = \sin\phi \ , \ b = \sin\chi \quad \left(-\frac{\pi}{2} \leqq \phi, \chi \leqq \frac{\pi}{2}\right)$$

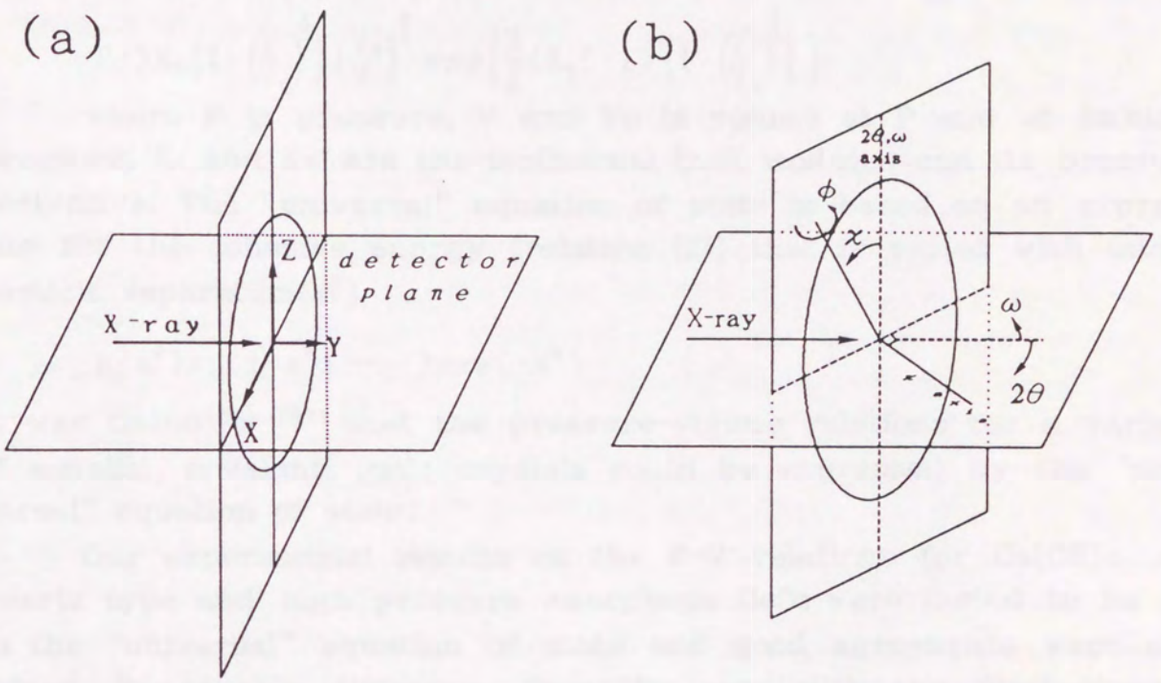

Fig.A-1 Schematic representation of a four-circle diffractometer. (a) The instrument with all angles set to zero (b) The positive direction of 2θ, ω, χ, ϕ rotation

Appendix 2

In the text, the Birch-Murnaghan's equation of state is used. The equation of state is based on finite-strain theory and known to be successful in matching previous compression data. On the other hand, Vinet et al.[55] proposed the "universal" equation of state having a following form (relation (1)).

$$P=3K_t\left\{1-\left(\frac{V}{V_0}\right)^{\frac{1}{3}}\right\}\left(\frac{V_0}{V}\right)^{\frac{2}{3}}\exp\left[\frac{3}{2}(K_t'-1)\left\{1-\left(\frac{V}{V_0}\right)^{\frac{1}{3}}\right\}\right] \quad (1)$$

where P is pressure, V and Vo is volume at P and at ambient pressure, K_t and K_t' are the isothermal bulk modulus and its pressure derivative. The "universal" equation of state is based on an expression for the cohesive energy (relation (2)) that is varied with inter-particle separation(a^*).

$$E(a^*)=-(1+a^*+\cdots\cdots)\exp(-a^*) \quad (2)$$

It was found[55]-[57] that the pressure-volume relations for a variety of metallic, covalent, ionic crystals could be expressed by the "universal" equation of state.

Our experimental results on the P-V relations for $Ca(OH)_2$, α-quartz type and high pressure amorphous GeO_2 were tested to be fit to the "universal" equation of state and good agreements were obtained. Remarkable difference from the case with the Birch-Murnaghan's equation of state was not seen (It was pointed out by Jeanloz[58] that the two equations of state gave almost same pressure for $\frac{V}{V_O}>0.6$). The determined K_t and K_t' are shown in Table A-1.

Table A-1 The bulk modulus and its pressure derivative determined with the "universal" equation of state and the Birch-Murnaghan's equation of state. (EOS stands for equation of state)

sample	(Birch-Murnaghan's EOS)		("universal" EOS)	
	K_t (GPa)	K_t'	K_t (GPa)	K_t'
$Ca(OH)_2$	30.4(2.4)	8.6(1.8)	30.6(2.5)	8.2(1.2)
q-GeO_2	32.7(3.3)	6.0(2.2)	32.6(3.3)	6.2(2.0)
Sample-13	52.2(0.3)	7.6(0.4)	52.1(0.3)	7.7(0.3)
Sample-14	60.4(0.4)	7.4(0.4)	60.4(0.4)	7.4(0.4)
Sample-20	76.6(0.9)	9.6(1.0)	76.6(0.9)	9.6(0.8)

Appendix 3

$LiKSO_4$ undergoes several phase transitions under low temperature. Its crystal structure is hexagonal belonging to the $P6_3$ space group at ambient temperature and pressure. A first-order phase transition has been observed at about 200 K by neutron diffraction experiment[59]. And nonlinear temperature variations of the dielectric constants of $LiKSO_4$ were observed at about 250 K and 200 K[60].

Our main purpose is to elucidate the possibility of the existence of the structural phase transition at about 250 K by X-ray diffraction experiment. Experiments were performed in a following procedure. Single-crystals of $LiKSO_4$ were grown by slow evaporation from aqueous solutions with equal stoichiometric concentrations of $Li_2SO_4 \cdot H_2O$ and K_2SO_4. In situ X-ray observations under low temperature (300-150 K) were performed by combining the PF system and a cryostat. A Mo target rotating anode X-ray generator was used under the condition of 50 kV and 50 mA. Pyrolytic graphite (002) reflection was utilized as monochrometor. The temperature of samples were controlled within $\pm$ 0.1 K. Temperature dependence of the line profile of the (401) reflection was precisely investigated (Fig.A-2). A new diffraction line appeared at the lower angle side of (401) reflection in 2θ at 200 K. The intensity of the new diffraction line increased with decreasing temperature. The first-order phase transition at about 200 K was observed as mentioned above (both reflections of the original and transformed phase were observed at 200 K). On the other hand, no remarkable change was observed at about 250 K. Therefore, we could not explain the anomaly of the dielectric constants at about 250 K with our experimental data. However, it was reported that a commensurate-incommmensurate phase transition occurred at about 230 K[61]. In the case where the anomaly of the dielectric constants is considered to be caused by the commensurate-incommensurate phase transition, superlattice reflections of the incommensurate phase are observed. In the present experiments, we have not confirmed the diffraction phenomenon yet.

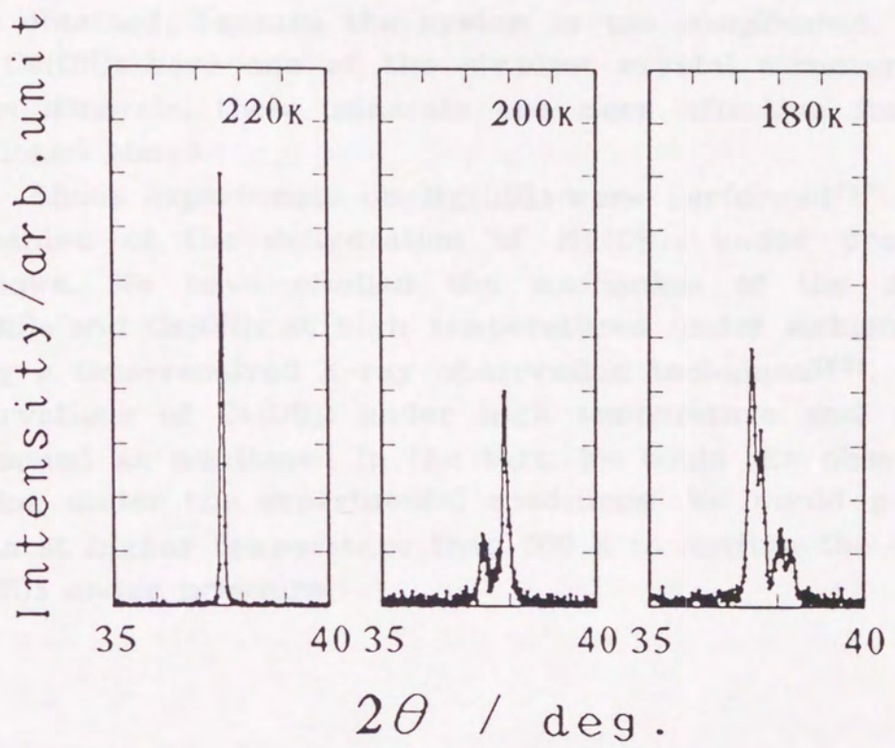

Fig.A-2 Change in the diffraction profile with decreasing temperature.

Appendix 4

Since phase transformations involving dehydration may be a source of deep seismicity in the mantle, the mechanism of the dehydration is an important study in earth science. Many investigators treated the $MgO-SiO_2-H_2O$ system to understand high pressure behavior of water in the mantle[62]. However, successful results have not been obtained, because the system is too complicated. Since $Mg(OH)_2$ and $Ca(OH)_2$ have one of the simplest crystal structures among hydrous minerals, these minerals are more effective for the purpose mentioned above.

Shock experiments on $Mg(OH)_2$ were performed[18]. However, the mechanism of the dehydration of $Mg(OH)_2$ under pressure is still unknown. We have studied the mechanism of the dehydration of $Mg(OH)_2$ and $Ca(OH)_2$ at high temperatures under ambient pressure by using a time-resolved X-ray observation technique[63]. In situ X-ray observations of $Ca(OH)_2$ under high temperature and pressure were performed as mentioned in the text. We could not observe the dehydration under the experimental conditions. We would perform experiments at higher temperature than 500 K to confirm the dehydration of $Ca(OH)_2$ under pressure.

Acknowledgment

The author would like to express his sincere thanks to Professors T.Yamanaka and S.Kume for their helpful guidance throughout this study and to Professor H.Takubo for his advice regarding preparation of the samples and discussions.

He also thanks Drs. Y.Miyamoto, I.Tanaka, E.Ito, K.Suito, I.Nakai and O.Ohtaka for usage of experimental facilities and discussions.

He also wishes to express thanks to Mr. M.Miyoshi for his kind instruction about the experiment and to Drs. S.Endo and R.Ohshima for their critical reading of this manuscript.

He also appreciates helpful discussions with all of the members in S.Kume's laboratory.

References

(1) Y.Fujii, M.Kowaka and A.Onodera: J. Phys. C 18 (1985) 789
(2) S.Sugai: J. Phys. C 18 (1985) 799
(3) R.J.Hemly, A.P.Jephcoat, H.K.Mao, L.C.Ming and M.H.Manghnani: Nature 334 (1988) 52
(4) M.B.Kruger and R.Jeanloz: Science 249 (1990) 647
(5) H.Sankaran, S.K.Sikca, S.M.Sharma and R.Chidambaran: Phys. Rev. B 38 (1988) 170
(6) Q.Williams, E.Knittle, R.Reichlin, S.Martin and R.Jeanloz: J. Geophys. Res. 95 (1990) 21549
(7) G.Richard and P.Richet: Geophys. Res. Lett. 17 (1990) 2093
(8) M.B.Kruger, Q.Williams and R.Jeanloz: J. Chem. Phys. 91 (1989) 5910
(9) J.P.Itie, A.Polian, G.Calas, J.Petiau, A.Fontaine and H.Tolentino: Phys. Rev. Lett. 63 (1989) 398
(10) Q.Williams and R.Jeanloz: Nature 338 (1989) 413
(11) J.R.Chelikowski, H.E.King,Jr., N.Troullier, J.L.Martins and J.Glinnemann: Phys. Rev. Lett. 65 (1990) 3309
(12) J.R.Chelikowski, N.Troullier, J.L.Martins and H.E.King,Jr.: Phys. Rev. B 44 (1991) 489
(13) H.Sowa: Zeitschrift fur Krist. 194 (1991) 291
(14) H.Sowa: Zeitschrift fur Krist. 184 (1988) 257
(15) O.Mishima, L.D.Calvert and E.Whalley: Nature 310 (1984) 393
(16) O.Mishima, L.D.Calvert and E.Whalley: Nature 314 (1985) 76
(17) F.Holuj and T.Kwan: J. Mag. Res. 18 (1975) 123
(18) T.S.Duffy, T.J.Ahrens, M.A.Lange and J.A.Tyburczy: Trans. Am. Geophys. Union 70 (1989) 1355
(19) L.Liu: "Elements, Oxides, and Silicates; High Pressure Phases with Implications for the Earth's Interior" Oxford University Press, New York (1988)
(20) G.S.Smith and P.B.Isaccs: Acta Cryst. 17 (1964) 842
(21) W.H.Baur and A.A.Khan: Acta Cryst. B 27 (1971) 2133
(22) V.G.Hill and L.Y.Chang: Am. Mineralogist 53 (1968) 1744
(23) J.D.Jorgensen: J. Appl. Phys. 49 (1978) 5473
(24) Y.Kudoh, H.Takeda and H.Arashi: Phys. Chem. Minerals 13 (1986) 233
(25) M.Sugiyama, S.Endo and K.Koto: Mineralogical Journal 13 (1987) 455
(26) Y.Yamada, M.Mori and Y.Noda: Solid State Comm. 32 (1979) 827
(27) H.Seto, Y.Noda and Y.Yamada: J. Phys. Soc. Jpn 57 (1988) 3668

(28) T.Yamanaka, S.Kawasaki and T.Shibata: "Advances in X-ray analysis" Plenum Press, New York, 35 (1992) in press
(29) W.R.Busing and H.A.Levy: Acta Cryst. 22 (1967) 457
(30) T.Sakurai: "A practical guide for X-ray crystal structure analysis" Syokabo, Tokyo (1983)
(31) S.Yamaoka, O.Fukunaga, O.Shimomura and H.Nakazawa: Rev. Sci. Instum. 50 (1979) 1163
(32) G.J.Piermarini, S.Block and J.D.Barnett: J. Appl. Phys. 44 (1973) 5377
(33) R.A.Forman, G.J.Piermarini, J.D.Barnett and S.Block: Science 176 (1972) 284
(34) H.K.Mao, J. Xu and P.M.Bell: J. Geophys. Res. 91 (1986) 4673
(35) S.Kawasaki, T.Yamanaka, S.Kume and T.Ashida: Solid State Comm. 76 (1990) 527
(36) F.Birch: J. Geophys. Res. 67 (1952) 227
(37) F.Birch: J. Geophys. Res. 83 (1978) 1257
(38) F.Holuj, M.Drozdowski and M.Czajkowski: Solid State Comm.: 56 (1985) 1019
(39) C.Meade and R.Jeanloz: Geophys. Res. Lett. 17 (1990) 1157
(40) R.Suyama, T.Ashida and S.Kume: J. Am. Ceram. Soc. 68 (1985) 314
(41) C.B.Finch and G.W.Clark: Am. Mineralogist 53 (1968) 1394
(42) L.Finger and H.King: Am. Mineralogist 63 (1978) 337
(43) R.M.Hazen. L.W.Finger, R.J.Hemly and H.K.Mao: Solid State Comm. 72 (1989) 507
(44) K.Suito, M.Miyoshi, T.Sasakura and H.Fujisawa: "High Pressure Research In Mineral Physics; Application to Earth and Planetary Science" Terra Scientific Publishing Company, Tokyo (1992) in press
(45) T.Sasakura, H.Yoneda, K.Suito and H.Fujisawa: High Pres. Res. 4 (1990) 318
(46) J.F.Scott: Phys. Rev. B 1 (1970) 3488
(47) P.F.McMillan and A.C.Hess: Phys. Chem. Minerals 17 (1990) 97
(48) G.H.Wolf, S.Wang, C.A.Herbst, D.J.Durben, F.Oliver, Z.C.Kang and K.Halvorson: "High Pressure Research In Mineral Physics; Application to Earth and Planetary Science" Terra Scientific Publishing Company, Tokyo (1992) in press
(49) B.Okai and J.Yoshimoto: J. Phys. Soc. Jpn 45 (1978) 1880
(50) B.Okai and J.Yoshimoto: J. Phys. Soc. Jpn 45 (1978) 1887
(51) C.Meade, R.Jeanloz and R.J.Hemly:"High Pressure Research In Mineral Physics; Application to Earth and Planetary Science" Terra Scientific Publishing Company, Tokyo (1992) in press
(52) R.M.Hazen and L.W.Finger: Phys. Chem. Solids 42 (1981) 143

(53) S.Tsuneyuki, Y.Matsui, H.Aoki and M.Tsukada: Nature 339 (1989) 209
(54) Y.Tsuchida and T.Yagi: Nature 347 (1990) 267
(55) P.Vinet, J.Ferrante, J.H.Rose and J.R.Smith: J. Geophys. Res. 92 (1987) 9319
(56) J.H.Rose, J.R.Smith and J.Ferrante: 28 (1983) 1835
(57) J.H.Rose, J.R.Smith, F.Guinea and J.Ferrante: Phys. Rev. B 29 (1984) 2963
(58) R.Jeanloz: Phys. Rev. B 38 (1988) 805
(59) S.Bhakay-Tamhane, A.Sequeria and R.Chidambaram: Solid State Comm. 53 (1985) 197
(60) T.Breczewski, T.Krajewski and B.Mroz: Ferroelectrics 33 (1981) 9
(61) C.H.A.Fonseca, G.M.Ribeiro, R.Gazzinelli and A.S.Chves: Solid State Comm. 46 (1983) 221
(62) M.Akaogi and S.Akimoto: Phys. Chem. Minerals 13 (1986) 161
(63) T.Yamanaka and T.Ashida: unpublished work